Two Peculiar Fast Transients in a Strongly Lensed Host Galaxy

S. A. RODNEY[1,] AND THE FRONTIERSN TEAM
Draft version December 13, 2016

ABSTRACT

Two unusual transient events were observed by the Hubble Space Telescope in 2014, appearing in a galaxy at z=1.0054±0.0002 that is gravitationally lensed by the galaxy cluster MACS J0416.1-2403. These transients—collectively nicknamed "Spock"—were faster and fainter than any supernova, but significantly more luminous than a classical nova: they reached peak luminosities of $\sim 10^{41}$ erg s^{-1} in $\lesssim 5$ rest-frame days, then faded below detectability in roughly the same timespan. Lens models of the foreground cluster suggest that it is entirely plausible that the two events are *spatially* coincident at the source plane, but very unlikely that they were also *temporally* coincident. We find that *Spock* can plausibly be classified as a recurrent nova, a luminous blue variable, or a stellar caustic crossing event—but all three explanations require either an extreme astrophysical source or highly unusual gravitational lensing.

1. INTRODUCTION

The Spock transient events—separately designated HFF14Spo-1 and HFF14Spo-2—appeared in Hubble Space Telescope (*HST*) imaging collected in January and August of 2014, respectively (Figure 1). These observations were centered on the galaxy cluster MACS J0416.1-2403 (hereafter, MACS0416) and were collected as part of the Hubble Frontier Fields (HFF) survey (HST-PID:13496, PI:Lotz), a multi-cycle program for deep imaging of 6 massive galaxy clusters and associated "blank sky" fields observed in parallel.

Combining the *HST* imaging and lens models of the MACS0416 gravitational lens leads to three key observables for the HFF14Spo events: (1) they are both more luminous than a classical nova, but less luminous than almost all supernovae (SNe), reaching a peak luminosity of roughly 10^{41} erg s[1] ($M_V = 14$); (2) both transients exhibited fast light curves, with rise and decline timescales of $\sim$2–5 days in the rest frame; and (3) it is likely that both events arose from the same physical location but were not coincident in time—they were probably separated by 3-5 months in the rest frame. These peculiar transients thus present an intriguing puzzle: they are broadly consistent with the expected behavior of stellar explosions (they each exhibit a single isolated rise and decline in brightness), but they can not be trivially classified into any of the common categories of explosive or eruptive astrophysical transients.

The HFF survey was not designed with the discovery of peculiar extragalactic transients as a core objective, but it has unintentionally opened an effective window of discovery for such events. Very faint sources at relatively high redshift ($z \gtrsim 1$) in these fields are made detectable by the substantial gravitational lensing magnification from the foreground galaxy clusters. Very rapidly evolving sources are also more likely to be found, due to the necessity of a rapid cadence for repeat imaging in the HFF program. These unusual characteristics for an *HST* survey enabled a precise measurement of the lensing

[1] Department of Physics and Astronomy, University of South Carolina, 712 Main St., Columbia, SC 29208, USA
srodney@sc.edu

magnification for SN Tomas, a high-redshift thermonuclear (Type Ia) SN (Rodney *et al.* 2015). The HFF imaging program also contributed to the detection and characterization of SN Refsdal, a high-redshift core-collapse SN and the first strongly-lensed SN observed with multiple resolved images (Kelly *et al.* 2015). The long-term monitoring campaign of SN Refsdal then led to the discovery of the peculiar lensed transient *Icarus*, which is posited to be a stellar caustic crossing event (Kelly *et al.* 2016). Even among this collection of rare transients, the HFF14Spo events appear to be *sui generis*. No single astrophysical model is clearly sufficient to explain all of the available observational data, and the best available models require either an extreme stellar source or a very unusual gravitational lensing configuration.

2. RESULTS

The two HFF14Spo events exhibited very similar light curves, as shown in Figure 2. Both events rose to a peak luminosity of $\sim$0.08 μJy and faded back to quiescence in < 20 days. The host galaxy for both HFF14Spo events is at a redshift of $z = 1.0054 \pm 0.0002$ (see Methods section 4.2). After dividing the observed timescales by $(1+z)$ to correct for cosmic time dilation, we see that both events exhibited a characteristic timescale of $\sim$2–5 days in the rest frame.

To interpret the observed light curves and the timing of these two events, we use six independently constructed cluster mass models to determine the effects of gravitational lensing from the MACS0416 cluster. As reported in Table 1, these lens models predict absolute magnification values between about $\mu = 10$ and $\mu = 100$ for both events. This wide range is due primarily to the close proximity of the HFF14Spo events to the lensing critical curve for sources at $z = 1$. Note that the magnifications for HFF14Spo-1 and HFF14Spo-2 are highly correlated. A variation of a given lens model that moves the critical curve closer to the position of HFF14Spo-1 would drive the magnification of that event much higher (toward $\mu_1 \sim 100$), but that would also have the effect of moving the critical curve farther from HFF14Spo-2 which would necessarily drive its magnification downward (toward $\mu_2 \sim 10$). From each model we also extract
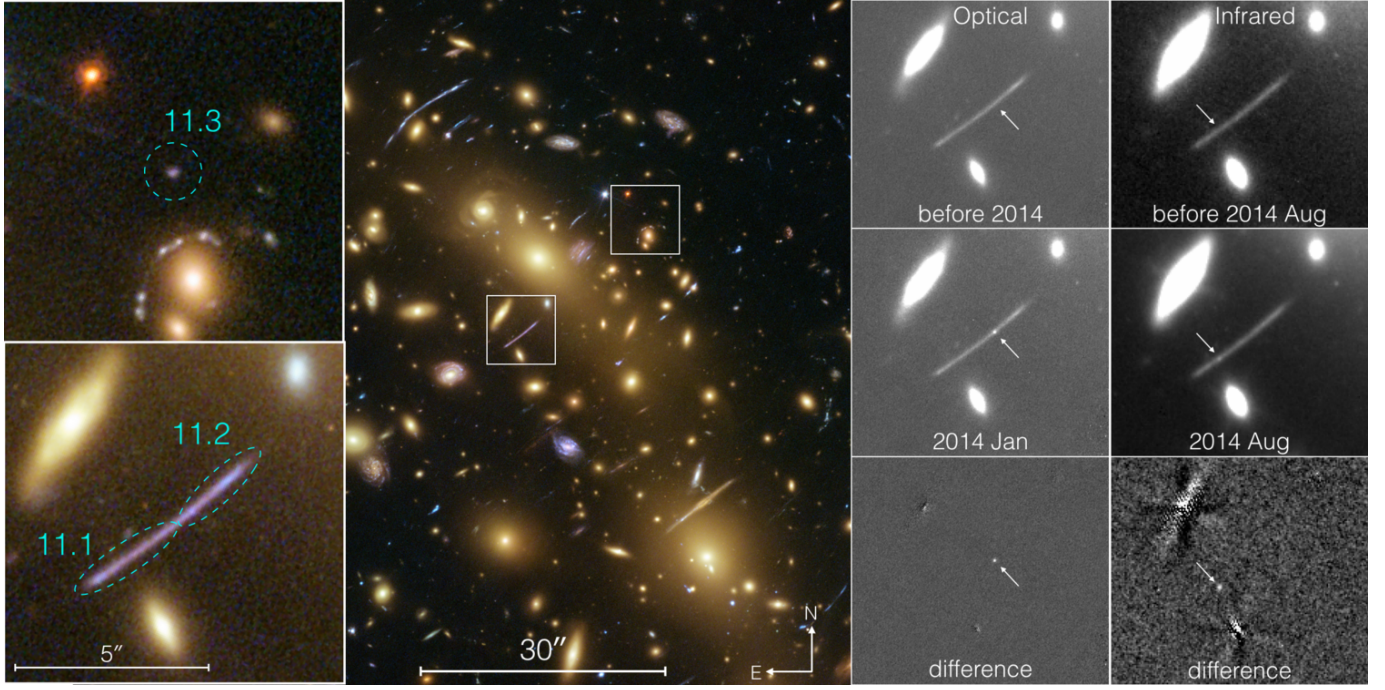
FIG. 1.— The detection of HFF14Spo-1 and HFF14Spo-2 in HST imaging from the Hubble Frontier Fields. The central panel shows the full field of the MACSJ0416 cluster, in a combined image using optical and infrared bands from HST. Two boxes within the main panel demarcate the regions where the HFF14Spo host galaxy images appear. These regions are shown as two inset panels on the left, highlighting the three images of the host galaxy (labeled 11.1, 11.2, and 11.3), whcih are caused by the gravitational lensing of the cluster. Two columns on the right side show the discovery of the two transient events in optical and infrared light, respectively. In these final two columns the top row is a template image, the center row shows the epoch when each transient appeared, and the bottom row is the difference image.
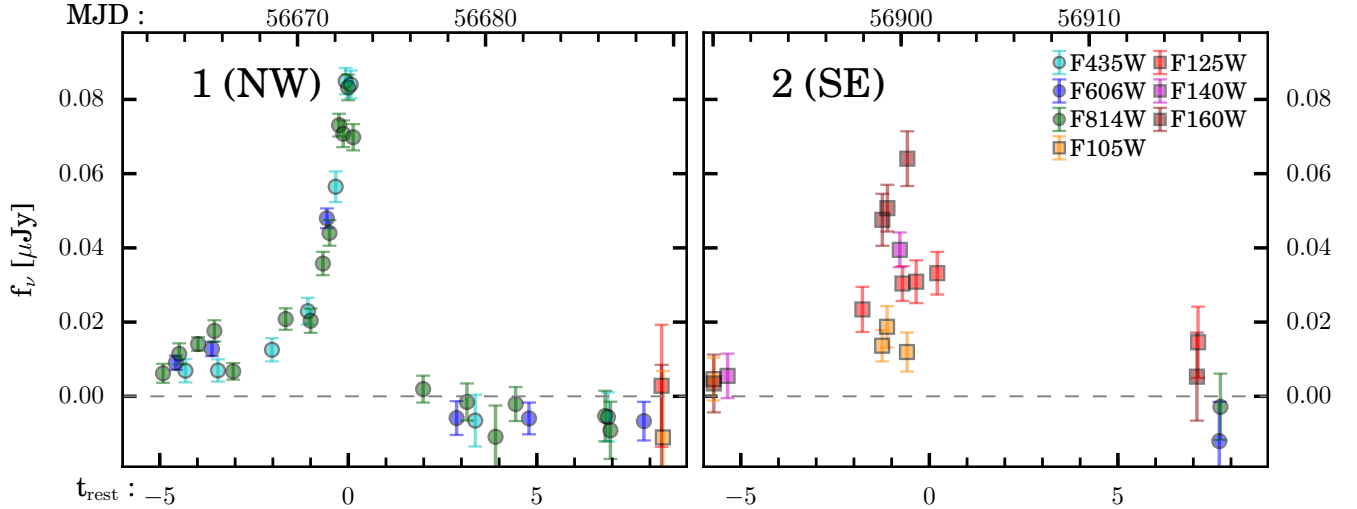

FIG. 2.— Light curves for the two transient events, HFF14Spo-1 on the left and HFF14Spo-2 on the right. Measured fluxes in micro-Janskys are plotted against rest-frame time at $z = 1.0054$, relative to the time of the peak observed flux for each event. The corresponding Mean Julian Date (MJD) in the observer frame is marked on the top axis for each panel. As indicated in the legend, optical observations using the HST ACS-WFC detector are plotted as circles in shades of blue and green, while infrared measurements from the WFC3-IR detector are plotted as red, orange and purple squares.
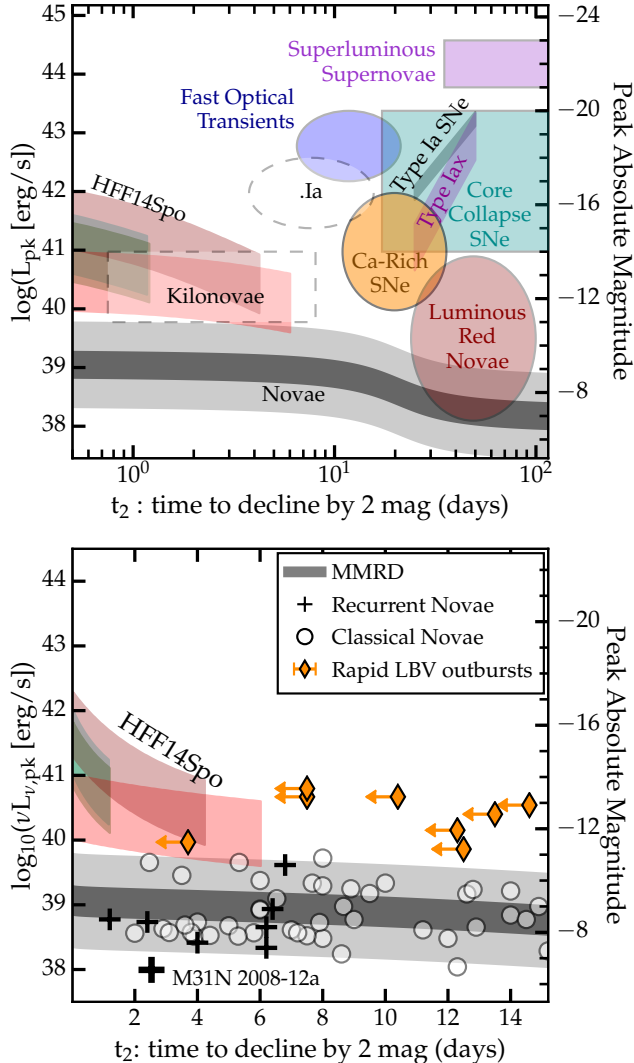
FIG. 3.— Peak luminosity vs. decline time for HFF14Spo and other rapidly declining recurrent transients. Constraints for HFF14Spo-1 and HFF14Spo-2 are plotted as overlapping colored bands, as in Figure ??. Grey bands show the MMRD relation for classical novae, as in Figure ??. Circles mark the observed peak luminosities and decline times for classical novae from the Milky Way (Downes and Duerbeck 2000), M31 (Shafter *et al.* 2011), and the local group (Kasliwal *et al.* 2011a). Black '+' symbols mark the 7 rapidly declining Recurrent Novae from our own galaxy (Schaefer 2010), and the large cross labeled at the bottom shows the rapid recurrence nova M31N 2008-12a (Tang *et al.* 2014; Darnley *et al.* 2015). Each orange diamond marks a separate short transient event from the two rapid LBV outburst systems, SN 2009ip (Pastorello *et al.* 2013) and NGC3432-LBV1 (a.k.a. SN 2000ch Pastorello *et al.* 2010). These LBV events provide only upper limits on the decline time due to limited photometric sampling.

two time delay predictions, given in Table 1. We report all time delays relative to the HFF14Spo-1 event, which appeared in January 2014 in host image 11.2.

2.1. *SNe and SN-like Transients*

A useful starting point for classification of optical transient events is to examine their position in the phase space of peak luminosity versus decline time (see, e.g., Kulkarni *et al.* 2007). We infer a range of plausible lumi-

TABLE 1
LENS MODEL PREDICTIONS FOR TIME DELAYS AND MAGNIFICATIONS.

Model	$\Delta t_{NW:SE}$ (days)	$\Delta t_{NW:11.3}$ (years)	μ_1	μ_2	μ_3
Bradac	42^{+13}_{-9}	-3.7 ± 0.3	90^{+61}_{-27}	32^{+8}_{-10}	$3.6^{+0.2}_{-0.5}$
Bradac-v3	$\cdots$	$\cdots$	38 ± 8	12.8 ± 0.8	2.9 ± 0.1
Diego	-48 ± 10	0.8	35 ± 20	30 ± 20	
Jauzac-A	29 ± 3	-2.2 ± 0.1	36^{+4}_{-3}	17 ± 1	4.5 ± 0.1
Jauzac-B	28^{+5}_{-7}	$-2.2^{+0.1}_{-0.2}$	37 ± 3	18 ± 2	4.6 ± 0.1
Jauzac-C	$2.5^{+0.8}_{-1.0}$	-3.0 ± 0.1	37^{+4}_{-3}	16^{+1}_{-2}	3.2 ± 0.05
Kawamata	$4.1^{+5.5}_{-3.4}$	$-5.0^{+0.5}_{-0.6}$	29^{+43}_{-10}	84^{+103}_{-38}	$3.0^{+0.2}_{-0.2}$
Williams	-10^{+1}_{-7}	$-2.5^{+1.0}_{-3.1}$	13^{+11}_{-6}	12^{+9}_{-5}	$3.1^{+2.2}_{-0.9}$
Zitrin	42^{+13}_{-9}	-3.7 ± 0.3	90^{+61}_{-27}	32^{+8}_{-10}	$3.6^{+0.2}_{-0.5}$

NOTE. — Each lens model is identified by the last name of the lead modeler or the principal investigator of the modeling team. Time delays give the predicted delay relative to an appearance in the NW host image, 11.2. Positive (negative) values indicate the NW image is the leading (trailing) image of the pair.

nosities and decline times for the HFF14Spo events using linear interpolation of the observed photometry, with corrections for the luminosity distance (assuming a standard ΛCDM cosmology), and accommodating the range of viable lensing magnifications ($10 < \mu < 100$) derived from the cluster lens models (Methods, 4.4). This results in two-dimensional constraints on L_{pk} and the decline timescale t_2 (the time over which the transient declines by 2 magnitudes). The HFF14Spo-1 and HFF14Spo-2 events are largely consistent with each other, and if both events are representative of a single system (or a homogeneous class) then the most likely peak luminosity and decline time (the region with the most overlap) would be $L_{pk} \sim 10^{41}$ ergs/s and $t_2 \sim 1.8$ days.

As shown in Figure 3, the relatively low peak luminosities and the very rapid rise and fall of both HFF14Spo light curves are incompatible with all of the common categories of stellar explosions. This includes the thermonuclear explosions of white dwarf stars as Type Ia SNe, and the heterogeneous class of massive star core collapse SNe. Less well-understood classes are also ruled out, such as Superluminous SNe (Gal-Yam 2012; Arcavi *et al.* 2016), Type Iax SNe (Foley *et al.* 2013), fast optical transients (Drout *et al.* 2014), Ca-rich SNe (Filippenko *et al.* 2003; Perets *et al.* 2011; Kasliwal *et al.* 2012), and Luminous Red Novae (also called intermediate luminosity red transients; Munari *et al.* 2002; Kulkarni *et al.* 2007; Kasliwal *et al.* 2011a).

The SN-like transients that come closest to matching the observed characteristics of the two HFF14Spo events are the "kilonova" class (also called a "macronova" or "mini-supernova") and the ".Ia" class. Kilonovae are a theorized category of optical transients that may be generated by the merger of a neutron star (NS) binary. Such a NS+NS merger can drive a relativistic jet that may be observed as a Gamma Ray Burst (GRB) and would emit gravitational waves. These may also be accompanied by a very rapid optical light curve (the kilonova component) that is driven by the radioactive decay of r-process ele-

ments in the ejecta (Li and Paczyński 1998; Kulkarni 2005). The .Ia class is due to He shell explosions that are expected to arise from AM Canum Venaticorum (AM CVn) binary star systems undergoing He mass transfer onto a white dwarf primary star (Warner 1995; Nelemans and Tout 2005; Bildsten *et al.* 2007). The HFF14Spo light curves exhibited a slower rise time than is expected for a kilonova event (e.g. Metzger *et al.* 2010; Barnes and Kasen 2013; Kasen *et al.* 2015), and a faster decline time than is anticipated for a .Ia event (Shen *et al.* 2010, e.g.). Furthermore, the HFF14Spo observations are not well matched by the few examples of observed kilonova candidates (Perley *et al.* 2009; Tanvir *et al.* 2013) or .Ia candidates (Kasliwal *et al.* 2010; Perets *et al.* 2010; Poznanski *et al.* 2010). However, there is enough uncertainty about the diversity of light curves generated by these rare explosions that we can not dismiss these models on the basis of light curve characteristics alone.

The primary reason to exclude any SN-like transient model is the problem of the apparent recurrence of the HFF14Spo events. For all of the catastrophic stellar explosions discussed so far, we do not expect to see repeated transient events. The SN and kilonova progenitor systems are completely disrupted at explosion. For .Ia events, even if we allow that an AM CVn system could produce repeated He shell flashes of similar luminosity, the period of recurrence would be of order 10^5 yr, making these effectively non-recurrent sources. Thus, the only way to reconcile these cataclysmic explosion models with the two observed HFF14Spo events is to either (a) assert that the two events are two images of the same explosion, appearing to us separately only because of a gravitational lensing time delay (as was the case for the 5 images of SN Refsdal Kelly *et al.* 2015, 2016), or (b) invoke a highly serendipitous occurrence of two unrelated peculiar explosions in the same host galaxy in the same year.

As shown in Table 1, none of the MACS0416 lens models predict an 8 month time delay between appearances in host galaxy images 11.1 and 11.2. To accept the first scenario (a) of a time-delayed single explosion, we would have to assume that a large systematic bias is similarly affecting all of the lens models. While we cannot rule out such a bias, the consistency of the lens modeling makes this scenario less tenable.

For the latter scenario (b) of two unrelated explosions, it is difficult to assess the likelihood of such an occurrence quantitatively, as there are no measured rates of .Ia or kilonovae. In a study of very fast optical transients with the Pan-STARRS1 survey, Berger *et al.* (2013) derived a limit of $\lesssim 0.05$ Mpc^{-3} yr^{-1} for transients reaching $M \approx -14$ mag on a timescale of ~ 1 day. This limit, though several orders of magnitude higher than the constraints on novae or SNe, is sufficient to make it exceedingly unlikely that two such transients would appear in the same galaxy in a single year. Furthermore, we have observed no other transients with similar luminosities and light curve shapes in high-cadence surveys of 5 other Frontier Fields clusters. Indeed, all other transients detected in the primary HFF survey have been fully consistent with normal SNe. Thus, we have no evidence to suggest that transients of this kind are common enough to be observed twice in a single galaxy in a single year.

2.2. *Luminous Blue Variable*

The transient sources categorized as Luminous Blue Variables (LBVs) are the result of eruptions or explosive episodes from massive stars ($> 10 M_\odot$). The class is exemplified by prototypical examples such as P Cygni, η Carinae (η Car), and S Doradus (S-Dor) (for recent overviews of the LBV class, see Smith *et al.* 2011; Kochanek *et al.* 2012). Although most giant LBV eruptions have been observed to last much longer than the HFF14Spo events (Smith *et al.* 2011), some LBVs have exhibited repeated rapid outbursts that are broadly consistent with the very fast HFF14Spo light curves. Because of this commonly seen stochastic variability, the LBV scenario does not have any trouble accounting for the HFF14Spo events as two separate episodes.

Two well-studied LBVs that provide a plausible match to the observed HFF14Spo events are "SN 2009ip" (Maza *et al.* 2009) and NGC3432-LBV1 (Pastorello *et al.* 2010). Both exhibited multiple brief transient episodes over a span of months to years (e.g., Miller *et al.* 2009; Li *et al.* 2009; Berger *et al.* 2009; Drake *et al.* 2010; Pastorello *et al.* 2010). Unfortunately, for these outbursts we have only upper limits on the decline timescale, t_2, due to the relatively sparse photometric sampling. Figure 3b shows that both HFF14Spo events are consistent with the observed luminosities and decline times of these fast and bright LBV outbursts – though the HFF14Spo events would be among the most rapid and most luminous LBV eruptions ever seen.

In addition to those relatively short and very bright giant eruptions, most LBVs also commonly exhibit a slower underlying variability. P Cygni and η Car, for example, slowly rose and fell in brightness by ~ 1 to 2 mag over a timespan of several years before and after their historic giant eruptions. Such variation has not been detected at the HFF14Spo locations. Nevertheless, given the broad range of light curve behaviors seen in LBV events, we can not reject this class as a possible explanation for the HFF14Spo system.

To explore some of the physical implications of an LBV classification for the two HFF14Spo events, we first make a rough estimate of the total radiated energy, which can be computed using the decline timescale t_2 and the peak luminosity $L_{\rm pk}$ following Smith *et al.* (2011):

$$E_{\rm rad} = \zeta t_2 L_{\rm pk}, \qquad (1)$$

where ζ is a factor of order unity that depends on the precise shape of the light curve.[2] Adopting $L_{\rm pk} \sim 10^{41}$ erg s^{-1} and $t_2 \sim 2$ days (as shown in Figure 3), we find that the total radiated energy isi $E_{\rm rad} \sim 10^{46}$ erg. A realistic range for this estimate would span $10^{44} < E_{\rm rad} < 10^{47}$ erg, due to uncertainties in the magnification, bolometric luminosity correction, decline time, and light curve shape (in roughly that order of importance). These uncertainties notwithstanding, our crude estimate does fall well within the range of plausible values for the total radiated energy of a major LBV outburst.

The precise physical mechanism for LBV outbursts is still not fully understood (e.g. Smith and Owocki 2006; Woosley *et al.* 2007; Dessart *et al.* 2010), but the canon-

---

[2] Note that Smith *et al.* (2011) used $t_{1.5}$ instead of t_2, which amounts to a different light curve shape term, ζ.

ical model is that LBV transient events are the optical signature of an eruptive mass loss episode. If this applies to the HFF14Spo transients, then the energy budget must also include a substantial amount of kinetic energy imparted to the ejected gas shell. Without spectroscopic information from the HFF14Spo transients we can not place any realistic estimate on the kinetic energy. Nevertheless, we can take the radiated energy as a rough lower limit on the total energy release and consider what timescale would be required for a massive star to build up that amount of energy (see Methods 4.9). This approach assumes that the energy released in an LBV eruption is generated slowly in the stellar interior and is in some way "bottled up" by the stellar envelope, before being released in a rapid mass ejection. By assuming that the build-up timescale is comparable to the rest-frame time between the two observed events, we estimate a quiescent luminosity of $L_{qui} \sim 10^{39.5}$ erg s-1 ($M_V \sim -10$). This value is fully consistent with the expected range for LBV progenitor stars (e.g., η Car has $M_V \sim -12$ and the faintest known LBV progenitors such as SN 2010dn have $M_V \sim -6$).

2.3. *Recurrent Nova*

Novae occur in binary systems in which a white dwarf star accretes matter from a less massive companion, leading to a burst of nuclear fusion in the accreted surface layer that causes the white dwarf to brighten by several orders of magnitude, but does not completely disrupt the star. In a recurrent nova (RN) system, the mass transfer from the companion to the white dwarf restarts after the explosion, so the cycle may begin again and repeat after a period of months or years.

The light curves of many RN systems in the Milky Way are similar in shape to the HFF14Spo episodes, exhibiting a sharp rise (< 10 days in the rest-frame) and a similarly rapid decline (see Methods section 4.10). This is reflected in Figure 3, where novae are represented by a grey band that traces the empirical constraints on the maximum magnitude - rate of decline (MMRD) relation for classical novae (Della Valle and Livio 1995; Downes and Duerbeck 2000; Shafter *et al.* 2011; Kasliwal *et al.* 2011b).

The RN model can provide a natural explanation for having two separate explosions that are coincident in space but not in time, as the two observed HFF14Spo events can be attributed to two distinct eruptions from the same RN system. However, the recurrence timescale for HFF14Spo in the rest-frame is 120 ± 30 days, which would be a singularly rapid recurrence period for a RN system. All RNe in our own galaxy have recurrence timescales ranging from 15–80 years (Schaefer 2010). The fastest measured recurrence timescale belongs to the Andromeda galaxy nova M31N 2008a-12, which has exhibited a new outburst every year from 2009-2015 (Tang *et al.* 2014; Darnley *et al.* 2014, 2015; Henze *et al.* 2015a,b). Although this M31 record-holder demonstrates that very rapid recurrence is possible, classifying HFF14Spo as a RN would still require a very extreme mass transfer rate to accommodate the < 1 year recurrence.

Another major concern with the RN hypothesis is that the two HFF14Spo events are substantially brighter than all known novae – perhaps by as much as 2 orders of magnitude. One might attempt to reconcile the HFF14Spo luminosity more comfortably with the nova class by assuming a significant lensing magnification for one of the two events. This would drive down the intrinsic luminosity, perhaps to $\sim 10^{40}$ erg s-1, on the edge of the nova region. However, this assumption implicitly moves the lensing critical curve to be closer to the HFF14Spo event in question. That pulls the critical curve away from the other HFF14Spo position, which makes that second event *more inconsistent* with observed nova peak luminosities.

The combination of a rapid recurrence timescale and unusually high peak luminosity for the HFF14Spo events is at odds with theoretical expectations and empirical constraints for RNe (see Methods section 4.11). Although the RN model is not strictly ruled out, we can deduce that if the HFF14Spo transients are caused by a single RN system, then that progenitor system would be the most extreme white dwarf binary system yet known.

2.4. *Microlensing*

In the presence of strong gravitational lensing it is possible to generate a transient event from lensing effects alone. In this case the background source has a steady luminosity but the relative motion of the source, lens, and observer causes the magnification of that source (and therefore the apparent brightness) to change rapidly with time. An isolated strong lensing event with a rapid timescale can be generated when a background star crosses over a lensing critical curve. In the case of a star crossing the caustic of a smooth lensing potential, the amplification of the source flux would increase (decrease) with a characteristic $t^{-1/2}$ profile as it moves toward (away from) the caustic. This slowly evolving light curve transitions to a very sharp decline (rise) when the star has moved to the other side of the caustic (Schneider and Weiss 1986; MiraldaEscude 1991). With a more complex lens comprising many compact objects, the light curve would exhibit a superposition of many such sharp peaks (Lewis *et al.* 1993). The peculiar transient *Icarus*, observed in another of the Hubble Frontier Fields, has been proposed as the first observed example of such a stellar caustic crossing event (P. Kelly et al., in prep).

The characteristic timescale of such a caustic crossing event would be on the order of hours or days (see Methods section 4.12), which is in the vicinity of the timescales observed for the HFF14Spo events. However, if we apply this scenario to the MACS0416 field, we can not plausibly generate two events with similar decay timescales at distinct locations on the sky. This is because a caustic-crossing transient event must necessarily appear at the location of the lensing critical curve, but in this case the lens models indicate that there is most likely a single critical curve that passes roughly mid-way between the two observed HFF14Spo locations.

Reasonable modifications of the MACS0416 lens models can allow for the possibility of multiple critical curves subtending the HFF14Spo host galaxy, so that instead of just two host images (11.1 and 11.2), the lensed galaxy arc is made up of 3 or more images of the host. This situation is disfavored on the grounds that the arc does not exhibit any gaps or bright features in the surface brightness profile. Furthermore, if multiple critical curves cross

the HFF14Spo host galaxy, it would be impossible to have a single star in the source plane be responsible for both of the HFF14Spo events. The angular separation of the two HFF14Spo events corresponds to a physical separation of many tens of parsecs in the source plane, and a star could not traverse that distance in the ∼120 rest-frame days that separate the two HFF14Spo events. With these considerations applied, a stellar caustic crossing could account for at best only one of the HFF14Spo events, not both.

2.5. *Non-explosive Astrophysical Transients*

There are several categories of astrophysical transients that are not related to stellar explosions, and we find that these models cannot accommodate the observations of the HFF14Spo transients. We may first dismiss any of the category of *periodic* sources (e.g. Cepheids, RR Lyrae, or Mira variables) that exhibit regular changes in flux due to pulsations of the stellar photosphere. These variable stars do not exhibit sharp, isolated transient episodes that could match the HFF14Spo light curve shapes. We can also rule out active galactic nuclei (AGN), in which brief transient episodes (a few days in duration) may be observed from X-ray to infrared wavelengths (e.g. Gaskell and Klimek 2003), principally due to the quiescence of the HFF14Spo sources between the two observed episodes and the absence of any of the broad emission lines that are often (though not always) observed in AGN. Stellar flares provide another very common source for optical transient events, but the total energy released by even the most extreme stellar flare falls far short of the observed energy release from the HFF14Spo transients (Balona 2012; Karoff *et al.* 2016) .

3. DISCUSSION

We have found that three models offer plausible explanations for the HFF14Spo events: (1) these transients are due to a RN that reaches an extraordinarily high peak luminosity, (2) they are separate rapid outbursts of an LBV star, or (3) they are each the result of the rapidly changing magnification of a massive star crossing over one or more lensing caustics. Our preferred explanation for the HFF14Spo events is that we have observed two distinct eruptive episodes from a massive LBV star. The light curve shape is consistent with rapid LBV eruptions seen in systems such as SN 2009ip and NGC 3432-LBV1. The peak luminosity and recurrence timescale are also within the bounds of what has been observed from nearby LBVs. The HFF14Spo episodes may have been among the fastest and most luminous of any rapid LBV events yet observed. However, the rapid outbursts of LBV stars in the local universe have never yet been observed with such a high cadence, so the detailed light curve shape of the HFF14Spo events can not be rigorously compared against other events. In this scenario, the HFF14Spo LBV system would most likely have exhibited multiple eruptions over the last few years, but most of them were missed, as they landed within the large gaps of the *HST* Frontier Fields imaging program.

We speculate that the very luminous and very fast HFF14Spo transients may be driven by extreme mass eruption events or an extreme form of stellar pulsation.

Both of these mechanisms are likely to occur in LBV progenitor stars, but there is not yet a consensus model that explains precisely how LBV eruptions are generated. This is a topic in need of significant theoretical work, with the end goal being a comprehensive physical model that accommodates both the η Car-like great eruptions and the S Dor-type variation of LBVs. The HFF14Spo events are extreme in several dimensions, and should add a useful benchmark for this theoretical challenge.

4. METHODS

4.1. *Discovery*

The transient HFF14Spo was discovered in HST imaging collected as part of the Hubble Frontier Fields (HFF) survey (HST-PID:13496, PI:Lotz), a multi-cycle program observing 6 massive galaxy clusters and associated "blank sky" parallel fields. Several HST observing programs have provided additional observations supplementing the core HFF program. One of these is the FrontierSN program (HST-PID:13386, PI:Rodney), which aims to identify and study explosive transients found in the HFF and related programs. The FrontierSN team discovered HFF14Spo in two separate HFF observing campaigns on the galaxy cluster MACS J0416.1-2403 (hereafter, MACS0416). The first was an imaging campaign in January, 2014 during which the MACS0416 cluster field was observed in optical bands using the Advanced Camera for Surveys Wide Field Camera (ACS-WFC). The second concluded in August, 2014, and imaged the cluster with the infrared detector of HST's Wide Field Camera 3 (WFC3-IR).

To discover transient sources, the FrontierSN team processes each new epoch of HST data through a difference imaging pipeline[3], using archival HST images to provide reference images (templates) which are subtracted from the astrometrically registered HFF images. In the case of MACS0416, the templates were constructed from images collected as part of the Cluster Lensing And Supernova survey with Hubble (CLASH, HST-PID:12459, PI:Postman). The resulting difference images are visually inspected for new point sources, and any new transients of interest (primarily supernovae, SNe) are followed up with additional HST imaging or ground-based spectroscopic observations as needed. For a more complete description of the operations of the FrontierSN program, see Rodney *et al.* (2015).

4.2. *Spectroscopy*

Spectroscopy of the HFF14Spo host galaxy was collected using three instruments on the Very Large Telescope (VLT). Observations with the VLT's X-shooter cross-dispersed echelle spectrograph (Vernet *et al.* 2011) were taken on October 19th, 21st and 23rd, 2014 (Program 093.A-0667(A), PI: J. Hjorth) with the slit centered on the position of HFF14Spo 2. The total integration time was 4.0 hours for the NIR arm of X-shooter, 3.6 hours for the VIS arm, and 3.9 hours for the UVB arm. The spectrum did not provide any detection of the transient source itself (as we will see below, it had already faded back to its quiescent state by that time). However, it did provide an unambiguous redshift for the host galaxy of $z = 1.0054 \pm 0.0002$ from Hα and the O[II] doublet in data from the NIR and VIS arms, respectively. These line identifications are consistent with two measures of the photometric redshift of the host: $z = 1.00 + -0.02$ from the BPZ algorithm (Benítez 2000), and $z = 0.92 \pm 0.05$, derived using the EAZY program (Brammer *et al.* 2008).

Additional VLT observations were collected using the Visible Multi-object Spectrograph (VIMOS Le Fèvre *et al.* 2003), as part of the CLASH-VLT large program (Program 186.A-0.798; P.I.: P. Rosati; Rosati *et al.* 2014)), which collected ∼4000 reliable redshifts over 600 arcmin^2 in the MACS J0416.1-2403 field (Grillo *et al.* 2015; Balestra *et al.* 2015). These massively multi-object observations could potentially have provided confirmation of the redshift of the HFF14Spo host galaxy with separate spectral line identifications in each of the three host galaxy images. On the MACS J0416.1-2403 field this program collected 1 hr of useful exposure time in good seeing conditions with the Low Resolution Blue grism. Unfortunately, the wavelength range of this grism (3600-6700 å) does not include any strong emission lines for a source at z=1.0054, and the signal-to-noise (S/N) was not sufficient to provide any clear line identifications for the three images of the HFF14Spo host galaxy.

The VLT Multi Unit Spectroscopic Explorer (MUSE; Henault *et al.* 2003; Bacon *et al.* 2012) observed the MACS J0416.1-2403 field as part of the SPECIFY PROGRAM INFO AND ADD CITATIONS HERE on DATES OF OBSERVATION AND EXPOSURE TIMES. These observations also confirmed the redshift of the host galaxy with clear detection of the O[II] doublet. Importantly, since MUSE is an integral field spectrograph, these observations also provided a confirmation of the redshift of the third image of the host galaxy, 11.3, with a matching O[II] line at the same wavelength.

A final source of spectroscopic information relevant to HFF14Spo is the Grism Lens Amplified Survey from Space (GLASS; PID: HST-GO-13459; PI:T. Treu Schmidt *et al.* 2014; Treu *et al.* 2015). The GLASS program collected slitless spectroscopy on the MACS J0416.1-2403 field using the WFC3-IR G102 and G141 grisms on *HST*. As with the VLT VIMOS data, the three sources identified as images of the HFF14Spo host galaxy are too faint in the GLASS data to provide any useful line identifications. There are also no other sources in the GLASS redshift catalog[4] that have a spectroscopic redshift consistent with z=1.0054.

4.3. *Photometry*

The follow-up observations for HFF14Spo included HST imaging observations in infrared and optical bands using the WFC3-IR and ACS-WFC detectors, respectively. Table **TODO:** (add a table with photometry) and Figure 2 present photometry of the HFF14Spo events from all available HST observations. The flux was measured on difference images, first using aperture photometry with a 0.″3 radius, and also by fitting with an empirical point spread function (PSF). The PSF model was defined using HST observations of the G2V standard star P330E, observed in a separate calibration program. A separate PSF model was defined for each filter, but owing to the long-term stability of the HST PSF we used the same model in all epochs. All of the aperture and PSF fitting photometry was carried out using the `PythonPhot` software package (Jones *et al.* 2015).

4.4. *Light Curve Fitting*

Due to the rapid decline timescale, no observations were collected for either event that unambiguously show the declining portion of the light curve. Therefore, we

---

[3] https://github.com/srodney/sndrizpipe
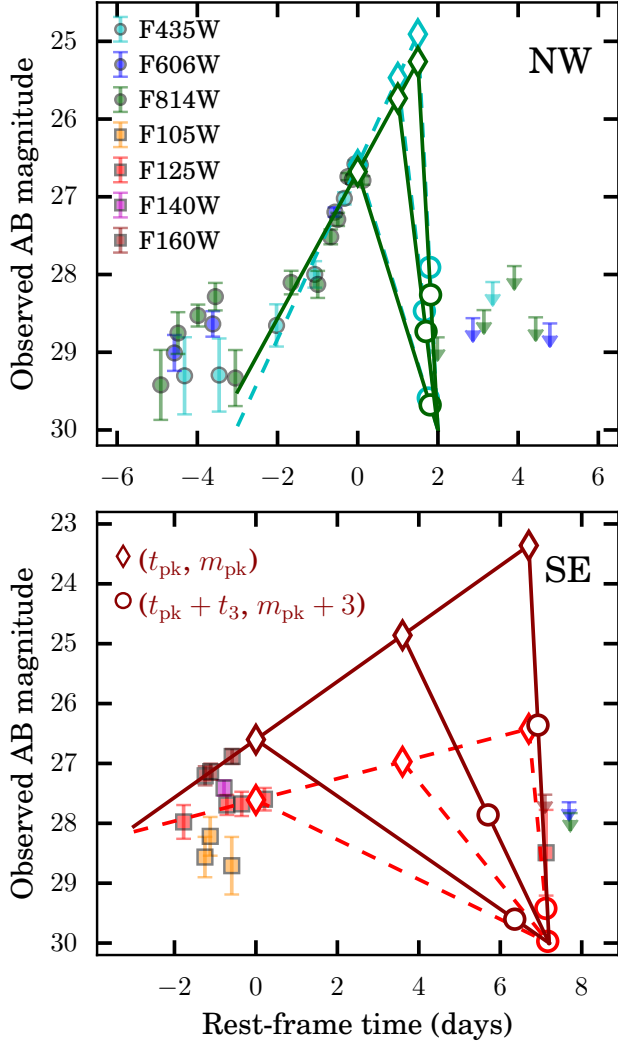
[4] http://glass.astro.ucla.edu/

FIG. 4.— Piece-wise linear fits to the HFF14Spo light curves, used to measure the rise time and decay time of the two events. The HFF14Spo-1 light curve is shown in the top panel, and HFF14Spo-2 in the bottom. Filled points with error bars plot the observed brightness of each event in AB magnitudes as a function of rest-frame time (for $z = 1.0054$). Piece-wise linear fits are shown for the four bands that have enough points for fitting: in the top panel fits are plotted for the F814W band (solid green lines) and the F435W band (dashed cyan lines), while in the bottom panel fits are shown for F160W (solid maroon) and F125W (dashed scarlet). Open diamonds in each panel show three examples of assumptions for the time of peak brightness, t_{pk} (i.e. the position where the rising piece of the linear fit ends). Open circles mark the corresponding point, $t_{pk} + t_3$, at which the fading transient would have declined in brightness by 3 magnitudes. See text for details on the fitting procedure.

must make some assumption for the shape of the light curve in order to quantify the peak luminosity and the corresponding timescales for the rise and the decline. We first approach this with a simplistic model that is piece-wise linear in magnitude vs time. Figure 4 shows examples of the resulting fits for the two events. For each fit we use only the data collected within 3 days of the brightest observed magnitude, which allows us to fit a linear rise separately for the F606W and F814W light curves for
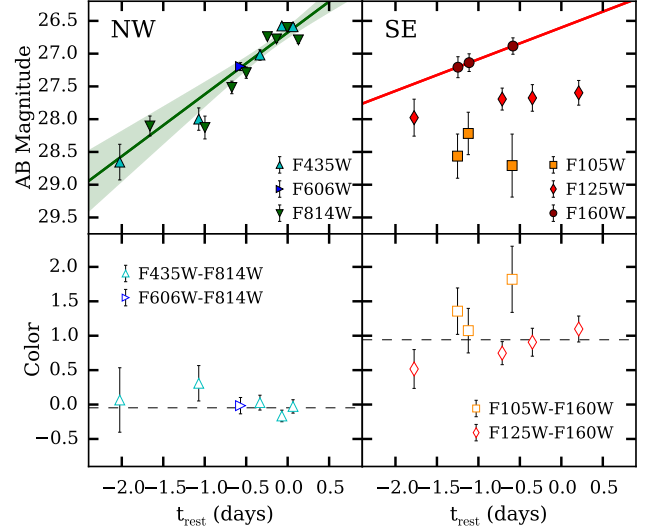

FIG. 5.— Observed colors for the HFF14Spo events. Filled points plotted in the top panels show observed AB magnitudes for the HFF14Spo-1 and HFF14Spo-2 events from -3 rest-frame days before the date of observed peak brightness. Solid lines and shaded regions show linear fits to the data in the F814W and F160W bands. Open points in the bottom panels show observed colors in the rest-frame bands. For each color the magnitude in the bluer band is the directly measured value, and the magnitude in the redder band is interpolated from the linear fits shown in the top panel. All colors are consistent with showing no evolution over the rising portion of each light curve.

HFF14Spo-1 and the F125W and F160W light curves for HFF14Spo-2. To quantify the covariance between the true peak brightness, the rise time and the decline timescale, we use the following procedure:

1. make an assumption for the date of peak, t_{pk};

2. measure the peak magnitude at t_{pk} from the linear fit to the rising light curve data;

3. assume the source reaches a minimum brightness (maximum magnitude) of 30 AB mag at the epoch of first observation after the peak;

4. draw a line for the declining light curve between the assumed peak and the assumed minimum brightness;

5. use that declining light curve line to measure the timescale for the event to drop by 2 magnitudes, t_2;

6. make a new assumption for t_{pk} and repeat.

As shown in Figure 4, the resulting piece-wise linear fits are simplistic, but nevertheless approximately capture the observed behavior for both events. Furthermore, since this toy model is not physically motivated, it allows us to remain agnostic for the time being as to the astrophysical source(s) driving these transients. From these fits we can see that HFF14Spo-1 most likely reached a peak magnitude between 25 and 26.5 AB mag in both F814W and F435W, and had a decline timescale t_2 of less than 2 days in the rest-frame. The observations of HFF14Spo-2 provide less stringent constraints, but we

see that it had a peak magnitude between 23 and 26.5 AB mag in F160W and exhibited a decline time of less than seven days. These fits also illustrate the generic fact that a higher peak brightness corresponds to a longer rise time and a faster decline timescale, independent of the specific model used. Changes to the arbitrary constraints we placed on these linear fits do not substantially affect the results. For example, the relationship between peak brightness and decline time is not strongly affected by adjusting the assumed maximum post-peak magnitude or changing the number of pre-peak data points used for the rising light curve fits.

At any assumed value for the time of peak brightness this linear interpolation gives an estimate of the peak magnitude. We then convert that to a luminosity (e.g., νL_ν in erg s^{-1}) by first correcting for the luminosity distance assuming a standard ΛCDM cosmology, and then accounting for an assumed lensing magnification, μ. The range of plausible lensing magnifications ($10 < \mu < 100$) is derived from the union of our six independent lens models (Methods, Figure 9). This results in a grid of possible peak luminosities for each event as a function of magnification and time of peak. As we are using linear light curve fits, the assumed time of peak is equivalent to an assumption for the decline time, which we quantify as t_2, the time over which the transient declines by 2 magnitudes.

4.5. Color Curves

At redshift $z = 1$ the observed optical and infrared bands translate to rest-frame ultraviolet (UV) and optical wavelengths, respectively. To derive rest-frame UV and optical colors from the observed photometry, we start with the measured magnitude in a relatively blue band (F435W and F606W for HFF14Spo-1 and F105W, F125W, F140W for HFF14Spo-2). We then subtract the coeval magnitude for a matched red band (F814W for HFF14Spo-1, F125W or F160W for HFF14Spo-2), derived from the linear fits to those bands. To adjust these to rest-frame filters, we apply K corrections (following Hogg *et al.* 2002), which we compute by defining a crude SED via linear interpolation between the observed broad bands for each transient event at each epoch. For consistency with past published results, we include in each K correction a transformation from AB to Vega-based magnitudes. The resulting UV and optical colors are plotted in Figure 5. Both HFF14Spo-1 and HFF14Spo-2 show little or no color variation over the period where color information is available.

4.6. Host Galaxy

To examine whether the two transients originated from the same physical location in the source plane, we looked for differences in the properties of the HFF14Spo host galaxy at the location of each event. We first used the technique of "pixel-by-pixel" SED fitting as described in Hemmati *et al.* (2014) to determine rest-frame colors and stellar properties in a single resolution element of the HST imaging data. For this purpose we used the deepest possible stacks of HST images, comprising all available data except those images where the transient events were present. The resulting maps of stellar population properties are shown in Figure 6. Table 2 reports measurements

TABLE 2
PROPERTIES OF THE LOCAL STELLAR POPULATION IN THE HFF14SPO HOST GALAXY, FROM SED FITTING.

Host image:	11.1	11.2	11.3
Location:	HFF14Spo-2	HFF14Spo-1	center
$(U - V)_{\rm rest}$	$0.69^{+0.2}_{-0.05}$	$0.52^{+0.15}_{-0.10}$	0.39 ± 0.05
$\log[\Sigma(M_*/{\rm M}_\odot)]$	7.14 ± 0.15	7.14 ± 0.15	7.04 ± 0.10
Age (Gyr)	0.292 ± 0.5	0.290 ± 0.5	0.292 ± 0.5

of the three derived stellar population properties (color, mass, age) from host images 11.1, 11.2 and 11.3. In 11.1 and 11.2 these measurements were extracted from the central pixel at the location of each of the two HFF14Spo events. Assuming the lensing magnification here ranges from $\mu = 10$ to 100 (see Section 4.7, this corresponds to a size on the source plane between 6 and 600 pc^2. For host image 11.3 we report the stellar population properties dervide from the pixel at the center of the galaxy. With a magnification of $\sim$3 to 5, the extraction region covers roughly 2000 to 6000 pc^2.

The reported uncertainties for these derived stellar properties in Table 2 reflect only the measurement errors from the SED fitting, and do not attempt to quantify potential systematic biases. Such biases could arise, for example, from color differences in the background light, which is dominated by the cluster galaxies and varies significantly across the MACS J0416.1-2403 field. Such a bias might shift the absolute values of the parameter scales for any given host image (e.g., making the galaxy as a whole appear bluer, more massive and younger). However, the gradients across any single host image are unlikely to be driven primarily by such systematics.

Figure 6 and Table 2 show that the measured values of the color, stellar mass, and age at the two HFF14Spo locations are mutually consistent. Thus, it is plausible to assume that the two positions map back to the same physical location at the source plane. Comparing those two locations to the center of the galaxy as defined in image 11.3, we see only a mild tension in the rest-frame U-V color. This comparison therefore can not quantitatively rule out the possibility that the two transient events are located at the center of the galaxy. However, the maps shown in Figure 6 do show a gradient in both U-V color and stellar age. For both images 11.1 and 11.2 the bluest and youngest stars (U-V$\sim$0.3, τ $\sim$280 Myr) are localized in knots near the extreme ends of each image, well separated from either of the HFF14Spo transient events. In the less distorted host image 11.3 the bluer and younger stars are concentrated near the center. Taken together, these color and age gradients suggest that the two transients are not coincident with the center of their host galaxy.

In addition to the HST imaging data, we also have spatially resolved spectroscopy from the MUSE integral field data. The only significant spectral line feature for the HFF14Spo host is the O[II] ($\lambda\lambda$ 3727, 3729) doublet, observed at 7474 and 7478 Å. Figure 7 shows the observed O[II] lines at 10 positions along the length of the arc, which comprises images 11.1 and 11.2. At each position the lines were extracted using apertures with a radius of 0.6″, so adjacent extractions are not independent, but extractions at the two HFF14Spo locations
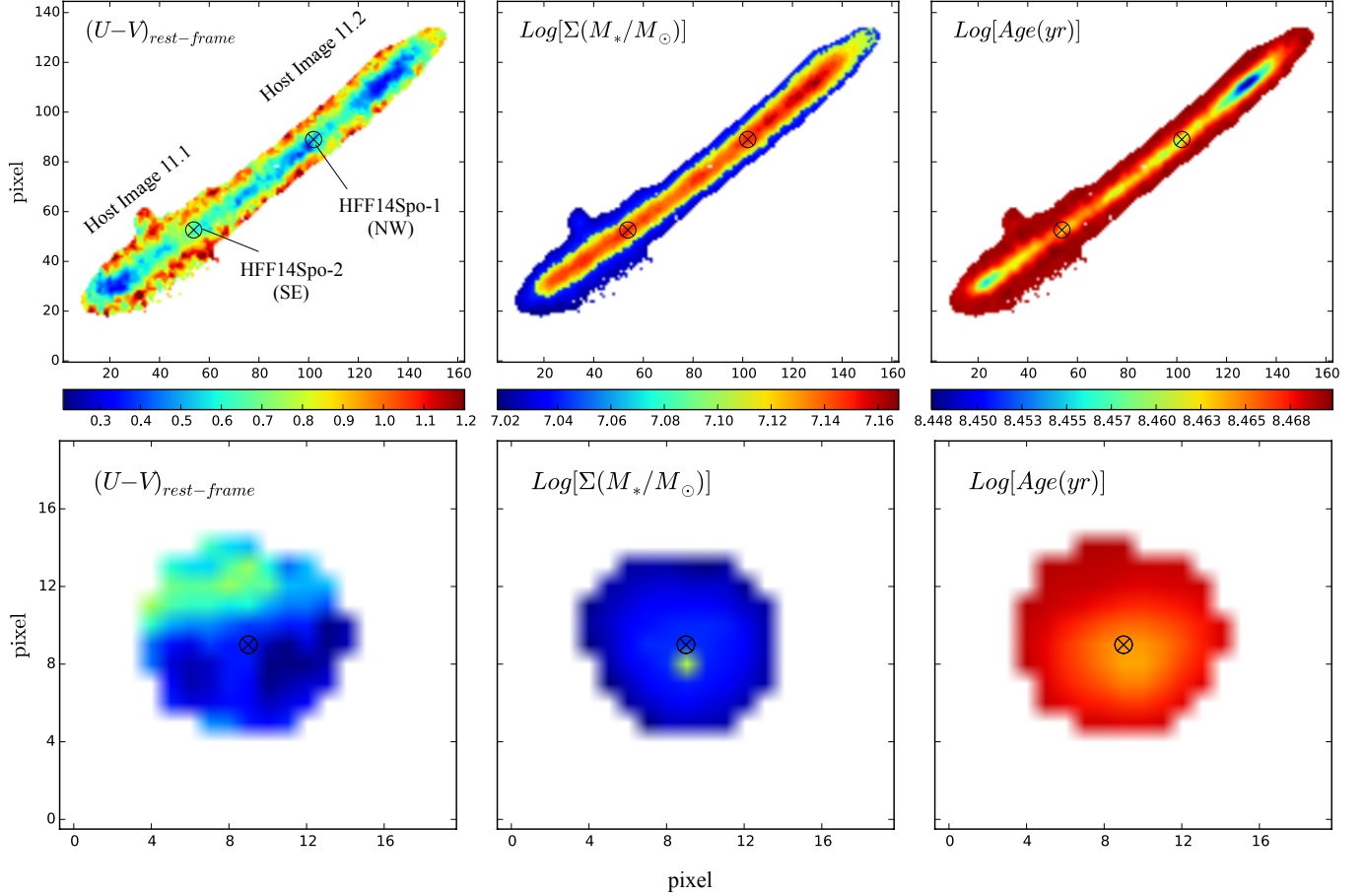
FIG. 6.— Stellar population properties of the HFF14Spo host galaxy, derived from "pixel-by-pixel" SED fitting. The top row shows maps for the adjacent host images 11.1 and 11.2, and the bottom panels show image 11.3. From left to right the panels present the rest-frame (U-V) color, the stellar surface mass density, Σ, and the mean age of the stellar population in Gyr. Markers in the top row denote the positions of the two HFF14Spo transient events. Markers in the bottom panels are at the center of host image 11.3.

have no overlap. Each extraction has been normalized to show a peak line flux at unity, so that the line profiles and the doublet line ratios may be more easily compared.

Properties derived from these line fits are reported in Table **??**. The O[II] lines do not exhibit any discernible gradient across the host galaxy images in terms of the wavelength of line centers, full width at half maximum, or the intensity ratio of the two components of the doublet. Thus, the O[II] measurements from MUSE can not be used to distinguish either HFF14Spo location from the other, or to definitively answer whether either position is coincident with the center of the host galaxy. We conclude that it is plausible but not certain that the two HFF14Spo events arose from the same physical location in the host galaxy.

4.7. Gravitational Lens Models

The five lens models used to provide estimates of the plausible range of magnifications and time delays are:
NOTE: THESE DESCRIPTIONS ARE PROBA-BLY INCORRECT. MODELERS, PLEASE FIX AS NEEDED.

- *Diego:* Created with the `WSLAP+` software (Sendra *et al.* 2014): Weak and Strong Lensing Analysis

Package plus member galaxies (Note: no weak-lensing constraints used for this MACS J0416 model). Interactive online model exploration available at `http://www.ifca.unican.es/users/jdiego/LensExplorer`.

- *Jauzac:* The model of Jauzac *et al.* (2014), generated with the `LENSTOOL` software (Jullo *et al.* 2007),[5] using strong- and weak-lensing constraints. This model makes a light-traces-mass assumption and parameterizes cluster components using Navarro-Frenk-White (NFW) density profiles (Navarro *et al.* 1997).

- *Kawamata:* The model of Kawamata *et al.* (2015), built using the `GLAFIC` software[6] with strong-lensing constraints.

- *Williams:* An adaptive grid model developed using the `GRALE` software tool (Liesenborgs *et al.* 2006, 2007; Mohammed *et al.* 2014), which uses a genetic algorithm to reconstruct the cluster mass profile

[5] `http://projects.lam.fr/repos/lenstool/wiki`
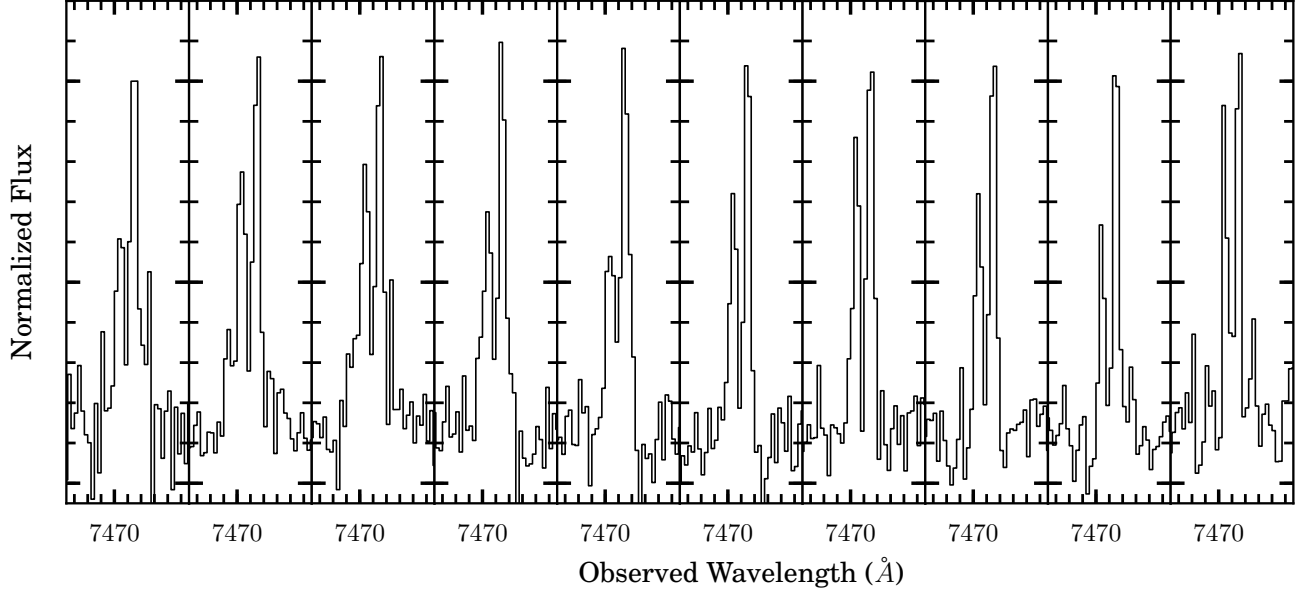[6] `http://www.slac.stanford.edu/~oguri/glafic/`

FIG. 7.— The [OII] line, observed with MUSE, at a series of ten locations along the HFF14Spo host galaxy arc. **TODO:** add in values for the [OII] doublet line ratio **TODO:** Add in panels showing [OII] lines from 11.3 and the spock locations. **TODO:** add in a panel showing the extraction apertures.
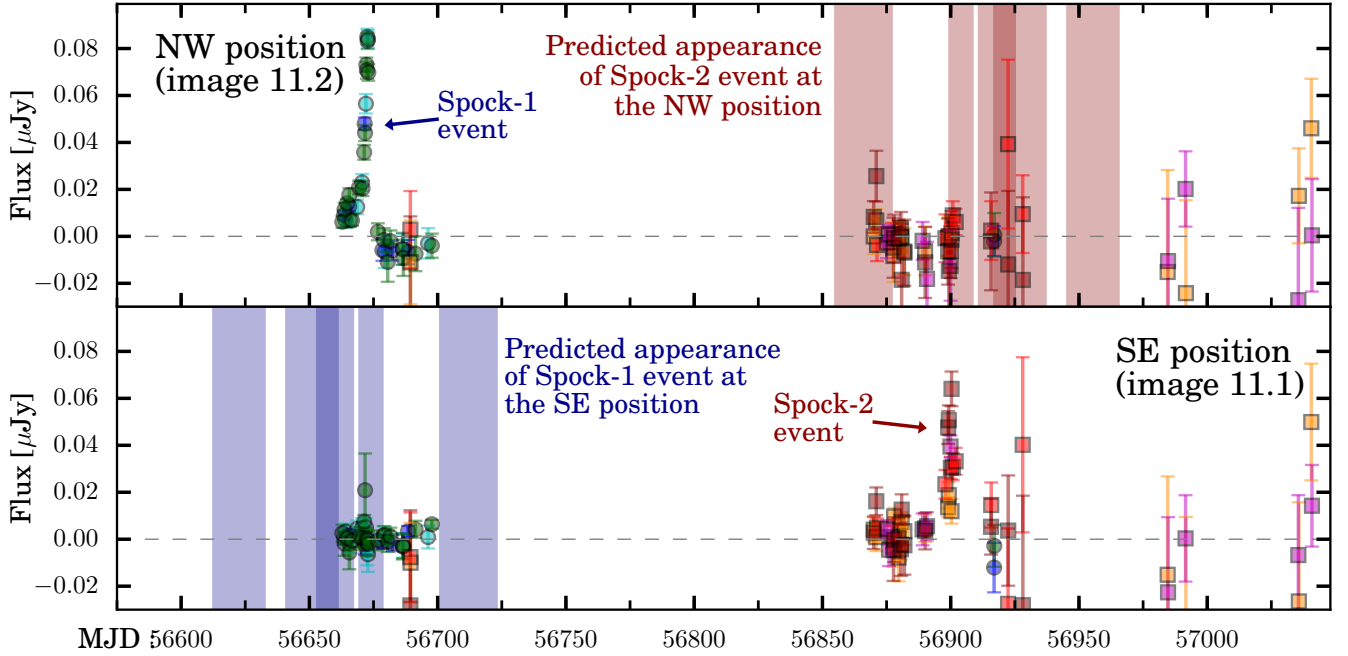

FIG. 8.— Predictions for the reappearance episodes of both HFF14Spo-1 and HFF14Spo-2 due to gravitational lensing time delays, as listed in Table 1. The top panel shows photometry collected at the NW position (host galaxy image 11.2) where the first event (HFF14Spo-1, labeled spock1) appeared in January, 2014. Optical measurements from ACS are in blue and green, and infrared observations from WFC3-IR are in red and orange, as in Figure 2. Each blue bar in the lower panel shows one lens model prediction for the dates when that same physical event (HFF14Spo-1) would have also appeared in the SE location (galaxy image 11.1), due to gravitational lensing time delay. The lower panel plots photometry from the SE position (11.1). On the right side we see the second observed event (HFF14Spo-2, labeled spock2). The red bars above show model predictions for when the NW host image 11.2 would have exhibited the gravitationally delayed image of the HFF14Spo-2 event. The width of each bar encompasses the 68% confidence region for a single model, and darker regions indicate an overlap from multiple models.

$$\mu_{\text{NW}} = 39\ ^{+56}_{-8}$$

$$\mu_{\text{SE}} = 22\ ^{+48}_{-5}$$

$$\mu_{11.3} = 3.8\ ^{+0.8}_{-0.7}$$

$$\Delta t_{\text{NW:SE}}\ [\text{days}] = 28\ ^{+13}_{-23}\ \text{days}$$

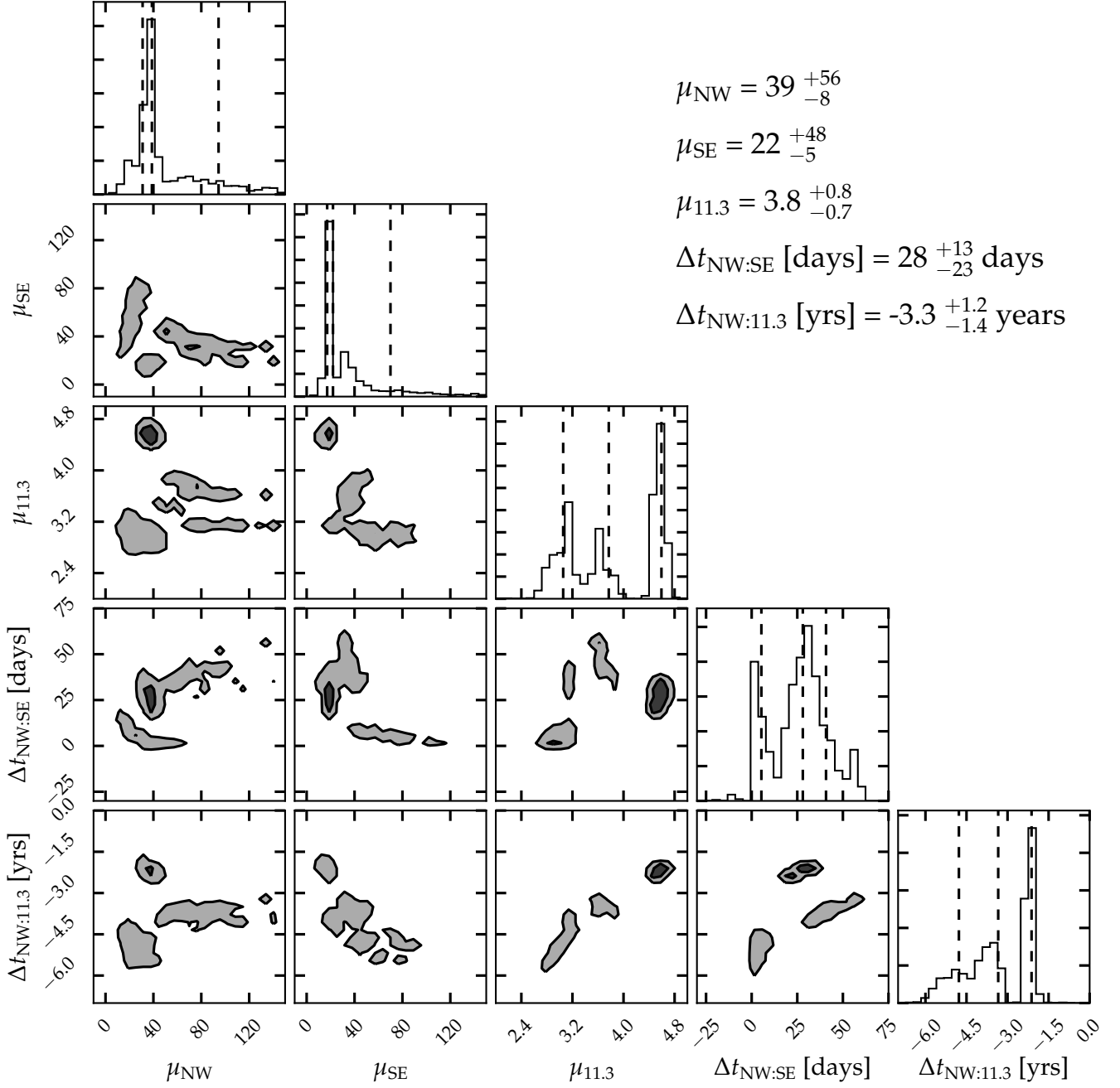$$\Delta t_{\text{NW:11.3}}\ [\text{yrs}] = -3.3\ ^{+1.2}_{-1.4}\ \text{years}$$

FIG. 9.— Probability distributions for the five primary magnification and time delay observables, drawn from a combination of results from four lens models. Contours shown in the ten panels at the lower left mark the 1-σ and 2-σ confidence regions in each 2D slice of the parameter space. Histograms at the top of each column show the marginalized 1D probability distributions, with dashed vertical lines marking the mean and 1σ confidence region. These mean values and uncertainties are also reported in the table of values at the upper right.

with an arrangement of projected Plummer 1911 density profiles.

- *Zitrin:* A model with strong- and weak-lensing constraints, built using the PIEMD+eNFW parameterization for density profiles as in Zitrin *et al.* (2009).

The *Williams* and *Zitrin* models were originally distributed as part of the Hubble Frontier Fields lens modeling project,[7] in which models were generated based on data available before the start of the HFF observations to enable rapid early investigations of lensed sources. The *Jauzac* model is an updated version of the model developed for that HFF modeling effort by the CATS team. In all cases the lens modelers made use of strong-lensing constraints (multiply-imaged systems and arcs) derived from HST imaging collected as part of the CLASH program (PI:Postman, HST PID:12459, Postman *et al.* 2012). These models also made use of spectroscopic redshifts in the cluster field from Mann and Ebeling (2012), Christensen *et al.* (2012), and Grillo *et al.* (2015). Input weak-lensing constraints also made use of data collected at the Subaru Telescope by PI K. Umetsu (in prep) and archival imaging. Priewe *et al.* (2016) provides a more complete description of the methodology of each model and a comparison of the magnification predictions and uncertainties across the entire MACS J0416.1-2403 field.

Figure 9 presents probability distributions derived from these models for the three magnifications and two time delay values of interest. These distributions were derived by combining the Monte Carlo chains from the Jauzac, Oguri, Williams and Zitrin models, with weighting applied to account for the different number of model iterations in each chain. Four of the five models agree that host image 11.3 is the leading image, appearing some 2–6 years before the other two images. The models do not agree on the arrival sequence of images 11.1 and 11.2: some have the NW image 11.2 as a leading image, and others have it as a trailing image. However, the models do consistently predict that the separation in time between those two images should be roughly in the range of 1 to 60 days.

4.8. *Luminous Blue Variable Light Curve Comparison*

Figure 10 presents a direct comparison of the observed HFF14Spo light curves against the light curves of the two LBVs that have well-studied rapid eruptions: SN 2009ip and NGC3432-LBV1. The brief outbursts of these LBVs have been less finely sampled than the two HFF14Spo events, but the available data show a wide variety of rise and decline times, even for a single object over a relatively narrow time window of a few months.

4.9. *LBV Build-up timescale*

The "build-up" timescale (Smith *et al.* 2011) matches the radiative energy released in an LBV eruption event with the radiative energy produced during the intervening quiescent phase:

[7] For more details, see https://archive.stsci.edu/prepds/frontier/lensmodels/

$$t_{\rm rad} = \frac{E_{\rm rad}}{L_{\rm qui}} = t_2 \frac{\xi L_{\rm pk}}{L_{\rm qui}}, \qquad (2)$$

where $L_{\rm qui}$ is the luminosity of the LBV progenitor star during quiescence.

The HFF14Spo events are not resolved as individual stars in their quiescent phase, so we have no useful constraint on the quiescent luminosity. Thus, instead of using a measured quiescent luminosity to estimate the build-up timescale, we assume that $t_{\rm rad}$ for HFF14Spo corresponds to the observed rest-frame lag between the two events, roughly 120 days (this accounts for both cosmic time dilation and a gravitational lensing time delay of ∼40 days). Adopting $L_{\rm pk} = 10^{41}$ erg s^{-1} and $t_2 = 2$ days (see Figure ??), we infer that the quiescent luminosity of the HFF14Spo progenitor would be $L_{\rm qui} \sim 10^{39.5}$ erg s−1 ($M_V \sim -10$).

4.10. *Recurrent Nova Light Curve Comparison*

There are ten known RNe in the Milky Way galaxy, and seven of these exhibit outbursts that decline rapidly, fading by two magnitudes in less than ten days (Schaefer 2010). Figure 11 compares the HFF14Spo light curves to a composite light curve (the gray shaded region), which encompasses the V band light curve templates (Schaefer 2010) for all seven of these galactic RN events. The Andromeda galaxy (M31) also hosts at least one RN with a rapidly declining light curve. The 2014 eruption of this well-studied nova, M31N 2008a-12, is shown as a solid black line in Figure 11, fading by 2 mags in less than 3 days. This comparison demonstrates that the rapid decline of both of the HFF14Spo transient events is fully consistent with the eruptions of known RNe in the local universe.

4.11. *Recurrent Nova Luminosity and Recurrence Period*

To examine the recurrence period and peak brightness of the HFF14Spo events relative to RNe, we rely on a pair of papers that evaluated an extensive grid of nova models through multiple cycles of outburst and quiescence (Prialnik and Kovetz 1995; Yaron *et al.* 2005). Figure 12 plots first the RN outburst amplitude (the apparent magnitude between outbursts minus the apparent magnitude at peak) and then the peak luminosity against the log of the recurrence period in years. For the HFF14Spo events we can only measure a lower limit on the outburst amplitude, since the presumed progenitor star is unresolved, so no measurement is available at quiescence. Figure 12 shows that a recurrence period as fast as one year is expected only for a RN system in which the primary WD is both very close to the Chandrasekhar mass limit (1.4 M$_\odot$) and also has an extraordinarily rapid mass transfer rate ($\sim 10^{-6}$ M$_\odot$ yr^{-1}). The models of Yaron *et al.* (2005) suggest that such systems should have a very low peak amplitude (barely consistent with the lower limit for HFF14Spo) and a low peak luminosity (∼100 times less luminous than the HFF14Spo events).

The closest analog for the HFF14Spo events from the population of known RN systems is the nova M31N 2008a-12. Kato *et al.* (2015) provided a theoretical model that can account for the key observational char-
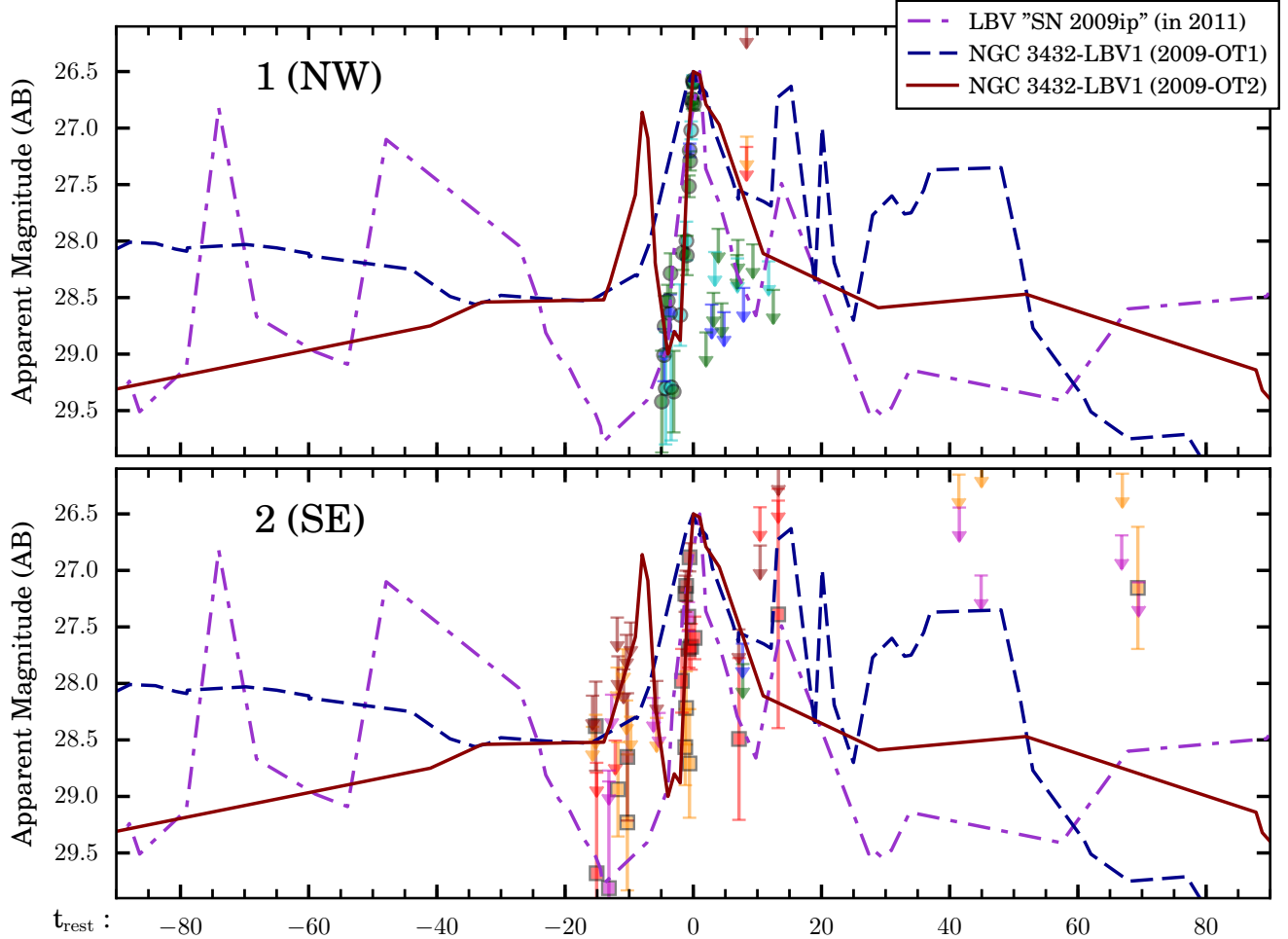
FIG. 10.— Comparison of observed HFF14Spo light curves against rapid outbursts from two LBVs.

acteristics of this remarkable nova: the very rapid recurrence timescale (<1 yr), fast optical light curve ($t_2 \sim 2$ days), and short supersoft x-ray phase (6-18 days after optical outburst Henze *et al.* 2015b). To match these observations, Kato *et al.* invoke a 1.38 $M_\odot$ white dwarf primary, drawing mass from a companion at a rate of 1.6×10^{-7} $M_\odot$ yr^{-1}. This is largely consistent with the theoretical expectations derived by Yaron *et al.* (2005), and reinforces the conclusion that a combination of a high mass white dwarf and efficient mass transfer are the key ingredients for rapid recurrence and short light curves. The one feature that can not be effectively explained with this scenario is the peculiarly high luminosity of the HFF14Spo events – even after accounting for the very large uncertainties.

4.12. *Expected Timescale for Microlensing Events*

A commonly observed example of microlensing-induced transient effects is when a bright background source (a quasar) by a galaxy-scale lens (Wambsganss 2001; Kochanek 2004). In this optically thick microlensing regime, the lensing potential along the line of sight to the quasar is composed of many stellar-mass objects. Each compact object along the line of sight generates a

separate critical lensing curve, resulting in a complex web of overlapping critical curves. As all of these lensing stars are in motion relative to the background source, the web of caustics will shift across the source position, leading to a stochastic variability on timescales of months to years. This scenario is inconsistent with the observed data, as the two HFF14Spo events were far too short in duration and did not exhibit the repeated "flickering" variation that would be expected from optically thick microlensing.

For the cluster-scale lens relevant in the case of HFF14Spo, we should expect to be in the optically thin microlensing regime. This situation is similar to the "local" microlensing light curves observed when stars within our galaxy or neighboring dwarf galaxies pass behind a massive compact halo object (Paczynski 1986; Alcock *et al.* 1993; Aubourg *et al.* 1993; Udalski *et al.* 1993). In this case, an isolated microlensing event can occur if there is a background star (i.e., in the HFF14Spo host galaxy) that is the dominant source of luminosity in its environment. In practice this means that the source must be a very bright O or B star with mass of order 10 $M_\odot$. Depending on its age, the size of such a star would range from a few to a few dozen times the size of the sun. The
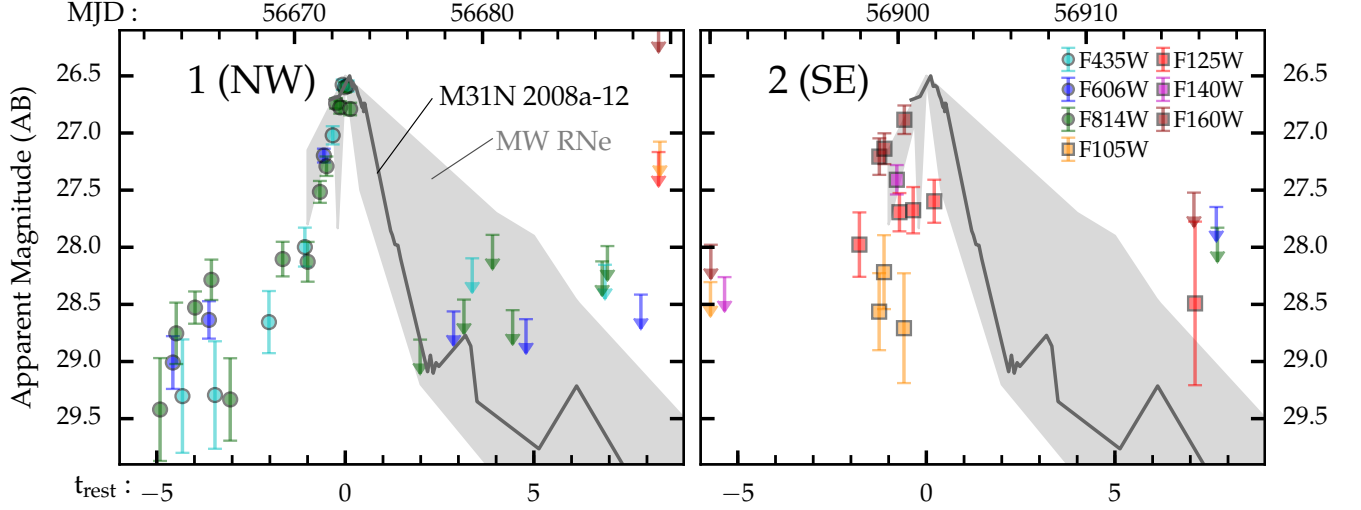
FIG. 11.— Comparison of the HFF14Spo light curves against template light curves for RN outbursts. Colored markers show the HFF14Spo light curve data, as in Figure 2, plotting the apparent magnitude as a function of time in the rest frame (bottom axis) and observer frame (top axis). The gray shaded regions encompass the outburst light curve shapes of 5 of the 11 known galactic RNe (U Sco, V2487 Oph, V394 CrA, T CrB, and V745 Sco), selected because they exhibit a rapid decline in their light curves (Schaefer 2010). The solid black line traces the 2014 outburst light curve shape for the rapid-recurrence nova M31N 2008a-12 (Darnley *et al.* 2014). All template light curves have been normalized to match the observed peaks of the HFF14Spo events.
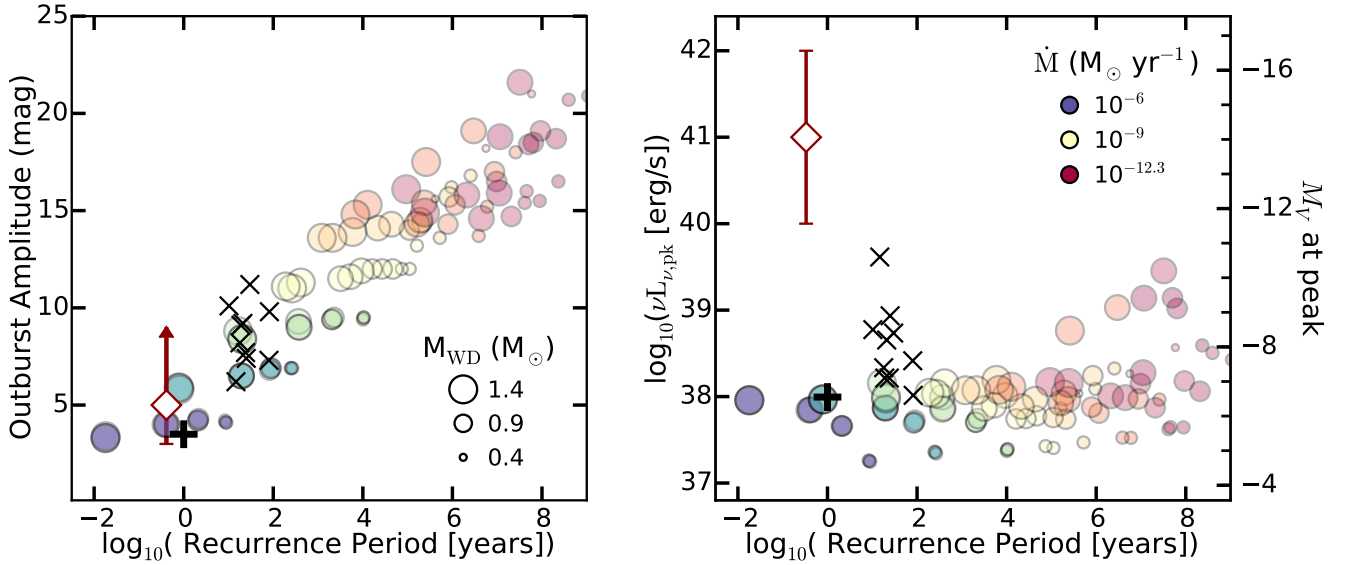

FIG. 12.— Comparison of the inferred HFF14Spo recurrence timescale against observed RNe and models. In the left panel the outburst amplitude in magnitudes is plotted against the recurrence timescale, while in the right panel the y axis shows the peak luminosity (or absolute magnitude). In both panels the joint constraints on HFF14Spo from both transient episodes are plotted as large open diamonds, observed constraints from the 10 galactic RNe appear as black 'x' points, and the rapid-recurrence nova M31N 2008a-12 is shown with a thick black '+' marker. Colored circles show the results from a suite of numerical hydrodynamic simulations from (Yaron *et al.* 2005). The size of each circle indicates the mass of the primary white dwarf (WD) star over the range 0.4-1.4 $M_\odot$, as indicated in the legend of the left panel. The color of each circle denotes the rate of mass transfer from the secondary onto the WD, as given in the right panel's legend.

net relative transverse velocity would be on the order of a few 100 km/s, which is comparable to the orbital velocity of stars within a galaxy or galaxies within a cluster.

In the case of a smooth cluster potential, the timescale τ for the light curve of such a caustic crossing event is dictated by the radius of the source, R, and the net transverse velocity, v, of the source across the caustic Chang

and Refsdal (1979, 1984); MiraldaEscude (1991):

$$\tau = 6 \frac{R}{5\,R_\odot} \frac{300\text{km s}^{-1}}{v} \text{ hr} \qquad (3)$$

Thus, for reasonable assumptions about the star's radius and velocity, the timescale τ is on the order of hours to days, which is well matched to the observed rise and decline timescales of the HFF14Spo events.

REFERENCES

S. A. Rodney, B. Patel, D. Scolnic, R. J. Foley, A. Molino, G. Brammer, M. Jauzac, M. Bradac, D. Coe, T. Broadhurst, J. M. Diego, O. Graur, J. Hjorth, A. Hoag, S. W. Jha, T. L. Johnson, P. Kelly, D. Lam, C. McCully, E. Medezinski, M. Meneghetti, J. Merten, J. Richard, A. Riess, K. Sharon, L.-G. Strolger, T. Treu, X. Wang, L. L. R. Williams, and A. Zitrin, ApJ, in press (2015).

P. L. Kelly, S. A. Rodney, T. Treu, R. J. Foley, G. Brammer, K. B. Schmidt, A. Zitrin, A. Sonnenfeld, L.-G. Strolger, O. Graur, A. V. Filippenko, S. W. Jha, A. G. Riess, M. Bradac, B. J. Weiner, D. Scolnic, M. A. Malkan, A. von der Linden, M. Trenti, J. Hjorth, R. Gavazzi, A. Fontana, J. C. Merten, C. McCully, T. Jones, M. Postman, A. Dressler, B. Patel, S. B. Cenko, M. L. Graham, and B. E. Tucker, Science **347**, 1123 (2015).

P. L. Kelly, S. A. Rodney, T. Treu, L.-G. Strolger, R. J. Foley, S. W. Jha, J. Selsing, G. Brammer, M. Bradač, S. B. Cenko, O. Graur, A. V. Filippenko, J. Hjorth, C. McCully, A. Molino, M. Nonino, A. G. Riess, K. B. Schmidt, B. Tucker, A. von der Linden, B. J. Weiner, and A. Zitrin, ApJ **819**, L8 (2016).

R. A. Downes and H. W. Duerbeck, AJ **120**, 2007 (2000).

A. W. Shafter, M. J. Darnley, K. Hornoch, A. V. Filippenko, M. F. Bode, R. Ciardullo, K. A. Misselt, R. A. Hounsell, R. Chornock, and T. Matheson, ApJ **734**, 12 (2011).

M. M. Kasliwal, S. R. Kulkarni, I. Arcavi, R. M. Quimby, E. O. Ofek, P. Nugent, J. Jacobsen, A. Gal-Yam, Y. Green, O. Yaron, D. B. Fox, J. L. Howell, S. B. Cenko, I. Kleiser, J. S. Bloom, A. Miller, W. Li, A. V. Filippenko, D. Starr, D. Poznanski, N. M. Law, G. Helou, D. A. Frail, J. D. Neill, K. Forster, D. C. Martin, S. P. Tendulkar, N. Gehrels, J. Kennea, M. Sullivan, L. Bildsten, R. Dekany, G. Rahmer, D. Hale, R. Smith, J. Zolkower, V. Velur, R. Walters, J. Henning, K. Bui, D. McKenna, and C. Blake, ApJ **730**, 134 (2011a).

B. E. Schaefer, ApJS **187**, 275 (2010).

S. Tang, L. Bildsten, W. M. Wolf, K. L. Li, A. K. H. Kong, Y. Cao, S. B. Cenko, A. De Cia, M. M. Kasliwal, S. R. Kulkarni, R. R. Laher, F. Masci, P. E. Nugent, D. A. Perley, T. A. Prince, and J. Surace, ApJ **786**, 61 (2014).

M. J. Darnley, M. Henze, I. A. Steele, M. F. Bode, V. A. R. M. Ribeiro, P. Rodríguez-Gil, A. W. Shafter, S. C. Williams, D. Baer, I. Hachisu, M. Hernanz, K. Hornoch, R. Hounsell, M. Kato, S. Kiyota, H. Kučáková, H. Maehara, J.-U. Ness, A. S. Piascik, G. Sala, I. Skillen, R. J. Smith, and M. Wolf, A&A **580**, A45 (2015).

A. Pastorello, E. Cappellaro, C. Inserra, S. J. Smartt, G. Pignata, S. Benetti, S. Valenti, M. Fraser, K. Takáts, S. Benitez, M. T. Botticella, J. Brimacombe, F. Bufano, F. Cellier-Holzem, M. T. Costado, G. Cupani, I. Curtis, N. Elias-Rosa, M. Ergon, J. P. U. Fynbo, F.-J. Hambsch, M. Hamuy, A. Harutyunyan, K. M. Ivarson, E. Kankare, J. C. Martin, R. Kotak, A. P. LaCluyze, K. Maguire, S. Mattila, J. Maza, M. McCrum, M. Miluzio, H. U. Norgaard-Nielsen, M. C. Nysewander, P. Ochner, Y.-C. Pan, M. L. Pumo, D. E. Reichart, T. G. Tan, S. Taubenberger, L. Tomasella, M. Turatto, and D. Wright, ApJ **767**, 1 (2013).

A. Pastorello, M. T. Botticella, C. Trundle, S. Taubenberger, S. Mattila, E. Kankare, N. Elias-Rosa, S. Benetti, G. Duszanowicz, L. Hermansson, J. E. Beckman, F. Bufano, M. Fraser, A. Harutyunyan, H. Navasardyan, S. J. Smartt, S. D. van Dyk, J. S. Vink, and R. M. Wagner, MNRAS **408**, 181 (2010).

S. R. Kulkarni, E. O. Ofek, A. Rau, S. B. Cenko, A. M. Soderberg, D. B. Fox, A. Gal-Yam, P. L. Capak, D. S. Moon, W. Li, A. V. Filippenko, E. Egami, J. Kartaltepe, and D. B. Sanders, Nature **447**, 458 (2007).

A. Gal-Yam, Science **337**, 927 (2012).

I. Arcavi, W. M. Wolf, D. A. Howell, L. Bildsten, G. Leloudas, D. Hardin, S. Prajs, D. A. Perley, G. Svirski, A. Gal-Yam, B. Katz, C. McCully, S. B. Cenko, C. Lidman, M. Sullivan, S. Valenti, P. Astier, C. Balland, R. G. Carlberg, A. Conley, D. Fouchez, J. Guy, R. Pain, N. Palanque-Delabrouille, K. Perrett, C. J. Pritchet, N. Regnault, J. Rich, and V. Ruhlmann-Kleider, ApJ **819**, 35 (2016).

R. J. Foley, P. J. Challis, R. Chornock, M. Ganeshalingam, W. Li, G. H. Marion, N. I. Morrell, G. Pignata, M. D. Stritzinger, J. M. Silverman, X. Wang, J. P. Anderson, A. V. Filippenko, W. L. Freedman, M. Hamuy, S. W. Jha, R. P. Kirshner, C. McCully, S. E. Persson, M. M. Phillips, D. E. Reichart, and A. M. Soderberg, ApJ **767**, 57 (2013).

M. R. Drout, R. Chornock, A. M. Soderberg, N. E. Sanders, R. McKinnon, A. Rest, R. J. Foley, D. Milisavljevic, R. Margutti, E. Berger, M. Calkins, W. Fong, S. Gezari, M. E. Huber, E. Kankare, R. P. Kirshner, C. Leibler, R. Lunnan, S. Mattila, G. H. Marion, G. Narayan, A. G. Riess, K. C. Roth, D. Scolnic, S. J. Smartt, J. L. Tonry, W. S. Burgett, K. C. Chambers, K. W. Hodapp, R. Jedicke, N. Kaiser, E. A. Magnier, N. Metcalfe, J. S. Morgan, P. A. Price, and C. Waters, ApJ **794**, 23 (2014).

A. V. Filippenko, R. Chornock, B. Swift, M. Modjaz, R. Simcoe, and M. Rauch, IAU Circ. **8159** (2003).

H. B. Perets, C. Badenes, I. Arcavi, J. D. Simon, and A. Gal-yam, ApJ **730**, 89 (2011).

M. M. Kasliwal, S. R. Kulkarni, A. Gal-Yam, P. E. Nugent, M. Sullivan, L. Bildsten, O. Yaron, H. B. Perets, I. Arcavi, S. Ben-Ami, V. B. Bhalerao, J. S. Bloom, S. B. Cenko, A. V. Filippenko, D. A. Frail, M. Ganeshalingam, A. Horesh, D. A. Howell, N. M. Law, D. C. Leonard, W. Li, E. O. Ofek, D. Polishook, D. Poznanski, R. M. Quimby, J. M. Silverman, A. Sternberg, and D. Xu, ApJ **755**, 161 (2012).

U. Munari, A. Henden, S. Kiyota, D. Laney, F. Marang, T. Zwitter, R. L. M. Corradi, S. Desidera, P. M. Marrese, E. Giro, F. Boschi, and M. B. Schwartz, A&A **389**, L51 (2002).

L.-X. Li and B. Paczyński, ApJ **507**, L59 (1998).

S. R. Kulkarni, ArXiv Astrophysics e-prints (2005).

B. Warner, Ap&SS **225**, 249 (1995).

G. Nelemans and C. A. Tout, MNRAS **356**, 753 (2005).

L. Bildsten, K. J. Shen, N. N. Weinberg, and G. Nelemans, ApJ **662**, L95 (2007).

B. D. Metzger, G. Martínez-Pinedo, S. Darbha, E. Quataert, A. Arcones, D. Kasen, R. Thomas, P. Nugent, I. V. Panov, and N. T. Zinner, MNRAS **406**, 2650 (2010).

J. Barnes and D. Kasen, ApJ **775**, 18 (2013).

D. Kasen, R. Fernández, and B. D. Metzger, MNRAS **450**, 1777 (2015).

K. J. Shen, D. Kasen, N. N. Weinberg, L. Bildsten, and E. Scannapieco, ApJ **715**, 767 (2010).

D. A. Perley, B. D. Metzger, J. Granot, N. R. Butler, T. Sakamoto, E. Ramirez-Ruiz, A. J. Levan, J. S. Bloom, A. A. Miller, A. Bunker, H.-W. Chen, A. V. Filippenko, N. Gehrels, K. Glazebrook, P. B. Hall, K. C. Hurley, D. Kocevski, W. Li, S. Lopez, J. Norris, A. L. Piro, D. Poznanski, J. X. Prochaska, E. Quataert, and N. Tanvir, ApJ **696**, 1871 (2009).

N. R. Tanvir, A. J. Levan, A. S. Fruchter, J. Hjorth, R. A. Hounsell, K. Wiersema, and R. L. Tunnicliffe, Nature **500**, 547 (2013).

M. M. Kasliwal, S. R. Kulkarni, A. Gal-Yam, O. Yaron, R. M. Quimby, E. O. Ofek, P. Nugent, D. Poznanski, J. Jacobsen, A. Sternberg, I. Arcavi, D. A. Howell, M. Sullivan, D. J. Rich, P. F. Burke, J. Brimacombe, D. Milisavljevic, R. Fesen, L. Bildsten, K. Shen, S. B. Cenko, J. S. Bloom, E. Hsiao, N. M. Law, N. Gehrels, S. Immler, R. Dekany, G. Rahmer, D. Hale, R. Smith, J. Zolkower, V. Velur, R. Walters, J. Henning, K. Bui, and D. McKenna, ApJ **723**, L98 (2010).

H. B. Perets, A. Gal-Yam, P. A. Mazzali, D. Arnett, D. Kagan, A. V. Filippenko, W. Li, I. Arcavi, S. B. Cenko, D. B. Fox, D. C. Leonard, D.-S. Moon, D. J. Sand, A. M. Soderberg, J. P. Anderson, P. A. James, R. J. Foley, M. Ganeshalingam, E. O. Ofek, L. Bildsten, G. Nelemans, K. J. Shen, N. N. Weinberg, B. D. Metzger, A. L. Piro, E. Quataert, M. Kiewe, and D. Poznanski, Nature **465**, 322 (2010).

D. Poznanski, R. Chornock, P. E. Nugent, J. S. Bloom, A. V. Filippenko, M. Ganeshalingam, D. C. Leonard, W. Li, and R. C. Thomas, Science **327**, 58 (2010).

E. Berger, C. N. Leibler, R. Chornock, A. Rest, R. J. Foley, A. M. Soderberg, P. A. Price, W. S. Burgett, K. C. Chambers, H. Flewelling, M. E. Huber, E. A. Magnier, N. Metcalfe, C. W. Stubbs, and J. L. Tonry, ApJ **779**, 18 (2013).

N. Smith, W. Li, J. M. Silverman, M. Ganeshalingam, and A. V. Filippenko, MNRAS **415**, 773 (2011).

C. S. Kochanek, D. M. Szczygieł, and K. Z. Stanek, ApJ **758**, 142 (2012).

J. Maza, M. Hamuy, R. Antezana, L. Gonzalez, P. Gonzalez, S. Lopez, G. Silva, *et al.*, CBET , 1 (2009).

A. A. Miller, W. Li, P. E. Nugent, J. S. Bloom, A. V. Filippenko, and A. T. Merritt, The Astronomer's Telegram **2183** (2009).

W. Li, N. Smith, A. A. Miller, and A. V. Filippenko, The Astronomer's Telegram **2212** (2009).

E. Berger, R. Foley, and I. Ivans, The Astronomer's Telegram **2184** (2009).

A. J. Drake, J. L. Prieto, S. G. Djorgovski, A. A. Mahabal, M. J. Graham, R. Williams, R. H. McNaught, M. Catelan, E. Christensen, E. C. Beshore, S. M. Larson, and S. Howerton, The Astronomer's Telegram **2897** (2010).

N. Smith and S. P. Owocki, ApJ **645**, L45 (2006).

S. E. Woosley, D. Kasen, S. Blinnikov, and E. Sorokina, ApJ **662**, 487 (2007).

L. Dessart, E. Livne, and R. Waldman, MNRAS **405**, 2113 (2010).

M. Della Valle and M. Livio, ApJ **452**, 704 (1995).

M. M. Kasliwal, S. B. Cenko, S. R. Kulkarni, E. O. Ofek, R. Quimby, and A. Rau, ApJ **735**, 94 (2011b).

M. J. Darnley, S. C. Williams, M. F. Bode, M. Henze, J.-U. Ness, A. W. Shafter, K. Hornoch, and V. Votruba, A&A **563**, L9 (2014).

M. Henze, M. J. Darnley, F. Kabashima, K. Nishiyama, K. Itagaki, and X. Gao, A&A **582**, L8 (2015a).

M. Henze, J.-U. Ness, M. J. Darnley, M. F. Bode, S. C. Williams, A. W. Shafter, G. Sala, M. Kato, I. Hachisu, and M. Hernanz, A&A **580**, A46 (2015b).

P. Schneider and A. Weiss, A&A **164**, 237 (1986).

J. MiraldaEscude, ApJ **379**, 94 (1991).

G. F. Lewis, J. Miralda-Escude, D. C. Richardson, and J. Wambsganss, MNRAS **261**, 647 (1993).

C. M. Gaskell and E. S. Klimek, Astronomical and Astrophysical Transactions **22**, 661 (2003).

L. A. Balona, MNRAS **423**, 3420 (2012).

C. Karoff, M. F. Knudsen, P. De Cat, A. Bonanno, A. Fogtmann-Schulz, J. Fu, A. Frasca, F. Inceoglu, J. Olsen, Y. Zhang, Y. Hou, Y. Wang, J. Shi, and W. Zhang, Nature Communications **7**, 11058 (2016).

J. Vernet, H. Dekker, S. D'Odorico, L. Kaper, P. Kjaergaard, F. Hammer, S. Randich, F. Zerbi, P. J. Groot, J. Hjorth, I. Guinouard, R. Navarro, T. Adolfse, P. W. Albers, J.-P. Amans, J. J. Andersen, M. I. Andersen, P. Binetruy, P. Bristow, R. Castillo, F. Chemla, L. Christensen, P. Conconi, R. Conzelmann, J. Dam, V. de Caprio, A. de Ugarte Postigo, B. Delabre, P. di Marcantonio, M. Downing, E. Elswijk, G. Finger, G. Fischer, H. Flores, P. François, P. Goldoni, L. Guglielmi, R. Haigron, H. Hanenburg, I. Hendriks, M. Horrobin, D. Horville, N. C. Jessen, F. Kerber, L. Kern, M. Kiekebusch, P. Kleszcz, J. Klougart, J. Kragt, H. H. Larsen, J.-L. Lizon, C. Lucuix, V. Mainieri, R. Manuputy, C. Martayan, E. Mason, R. Mazzoleni, N. Michaelsen, A. Modigliani, S. Moehler, P. Møller, A. Norup Sørensen, P. Nørregaard, C. Péroux, F. Patat, E. Pena, J. Pragt, C. Reinero, F. Rigal, M. Riva, R. Roelfsema, F. Royer, G. Sacco, P. Santin, T. Schoenmaker, P. Spano, E. Sweers, R. Ter Horst, M. Tintori, N. Tromp, P. van Dael, H. van der Vliet, L. Venema, M. Vidali, J. Vinther, P. Vola, R. Winters, D. Wistisen, G. Wulterkens, and A. Zacchei, A&A **536**, A105 (2011).

N. Benítez, ApJ **536**, 571 (2000).

G. B. Brammer, P. G. van Dokkum, and P. Coppi, ApJ **686**, 1503 (2008).

O. Le Fèvre, M. Saisse, D. Mancini, S. Brau-Nogue, O. Caputi, L. Castinel, S. D'Odorico, B. Garilli, M. Kissler-Patig, C. Lucuix, G. Mancini, A. Pauget, G. Sciarretta, M. Scodeggio, L. Tresse, and G. Vettolani, in *Instrument Design and Performance for Optical/Infrared Ground-based Telescopes*, Society of Photo-Optical Instrumentation Engineers (SPIE) Conference Series, Vol. 4841, edited by M. Iye and A. F. M. Moorwood (2003) pp. 1670–1681.

P. Rosati, I. Balestra, C. Grillo, A. Mercurio, M. Nonino, A. Biviano, M. Girardi, E. Vanzella, and Clash-VLT Team, The Messenger **158**, 48 (2014).

C. Grillo, S. H. Suyu, P. Rosati, A. Mercurio, I. Balestra, E. Munari, M. Nonino, G. B. Caminha, M. Lombardi, G. De Lucia, S. Borgani, R. Gobat, A. Biviano, M. Girardi, K. Umetsu, D. Coe, A. M. Koekemoer, M. Postman, A. Zitrin, A. Halkola, T. Broadhurst, B. Sartoris, V. Presotto, M. Annunziatella, C. Maier, A. Fritz, E. Vanzella, and B. Frye, ApJ **800**, 38 (2015).

I. Balestra, A. Mercurio, B. Sartoris, M. Girardi, C. Grillo, M. Nonino, P. Rosati, A. Biviano, S. Ettori, W. Forman, C. Jones, A. Koekemoer, E. Medezinski, G. A. Ogrean, P. Tozzi, K. Umetsu, E. Vanzella, R. J. van Weeren, A. Zitrin, M. Annunziatella, G. B. Caminha, T. Broadhurst, D. Coe, M. Donahue, A. Fritz, B. Frye, D. Kelson, M. Lombardi, C. Maier, M. Meneghetti, A. Monna, M. Postman, M. Scodeggio, S. Seitz, and B. Ziegler, ArXiv e-prints (2015).

F. Henault, R. Bacon, C. Bonneville, D. Boudon, R. L. Davies, P. Ferruit, G. F. Gilmore, O. Le Fèvre, J.-P. Lemonnier, S. Lilly, S. L. Morris, E. Prieto, M. Steinmetz, and P. T. de Zeeuw, in *Instrument Design and Performance for Optical/Infrared Ground-based Telescopes*, Proc. SPIE, Vol. 4841, edited by M. Iye and A. F. M. Moorwood (2003) pp. 1096–1107.

R. Bacon, M. Accardo, L. Adjali, H. Anwand, S.-M. Bauer, J. Blaizot, D. Boudon, J. Brinchmann, L. Brotons, P. Caillier, L. Capoani, M. Carollo, M. Comin, T. Contini, C. Cumani, E. Daguis, S. Deiries, B. Delabre, S. Dreizler, J.-P. Dubois, M. Dupieux, C. Dupuy, E. Emsellem, A. Fleischmann, M. François, G. Gallou, T. Gharsa, N. Girard, A. Glindemann, B. Guiderdoni, T. Hahn, G. Hansali, D. Hofmann, A. Jarno, A. Kelz, M. Kiekebusch, J. Knudstrup, C. Koehler, W. Kollatschny, J. Kosmalski, F. Laurent, M. Le Floch, S. Lilly, J.-L. Lizon à L'Allemand, M. Loupias, A. Manescau, C. Monstein, H. Nicklas, J. Niemeyer, J.-C. Olaya, R. Palsa, L. Parès, L. Pasquini, A. Pécontal-Rousset, R. Pello, C. Petit, L. Piqueras, E. Popow, R. Reiss, A. Remillieux, E. Renault, P. Rhode, J. Richard, J. Roth, G. Rupprecht, J. Schaye, E. Slezak, G. Soucail, M. Steinmetz, O. Streicher, R. Stuik, H. Valentin, J. Vernet, P. Weilbacher, L. Wisotzki, N. Yerle, and G. Zins, The Messenger **147**, 4 (2012).

K. B. Schmidt, T. Treu, G. B. Brammer, M. Bradač, X. Wang, M. Dijkstra, A. Dressler, A. Fontana, R. Gavazzi, A. L. Henry, A. Hoag, T. A. Jones, P. L. Kelly, M. A. Malkan, C. Mason, L. Pentericci, B. Poggianti, M. Stiavelli, M. Trenti, A. von der Linden, and B. Vulcani, ApJ **782**, L36 (2014).

T. Treu, K. B. Schmidt, G. B. Brammer, B. Vulcani, X. Wang, M. Bradač, M. Dijkstra, A. Dressler, A. Fontana, R. Gavazzi, A. L. Henry, A. Hoag, K.-H. Huang, T. A. Jones, P. L. Kelly, M. A. Malkan, C. Mason, L. Pentericci, B. Poggianti, M. Stiavelli, M. Trenti, and A. von der Linden, ApJ **812**, 114 (2015).

D. O. Jones, D. M. Scolnic, and S. A. Rodney, "PythonPhot: Simple DAOPHOT-type photometry in Python," Astrophysics Source Code Library (2015).

D. W. Hogg, I. K. Baldry, M. R. Blanton, and D. J. Eisenstein, ArXiv Astrophysics e-prints (2002).

S. Hemmati, S. H. Miller, B. Mobasher, H. Nayyeri, H. C. Ferguson, Y. Guo, A. M. Koekemoer, D. C. Koo, and C. Papovich, ApJ **797**, 108 (2014).

I. Sendra, J. M. Diego, T. Broadhurst, and R. Lazkoz, MNRAS **437**, 2642 (2014).

M. Jauzac, B. Clément, M. Limousin, J. Richard, E. Jullo, H. Ebeling, H. Atek, J.-P. Kneib, K. Knowles, P. Natarajan, D. Eckert, E. Egami, R. Massey, and M. Rexroth, MNRAS **443**, 1549 (2014).

E. Jullo, J.-P. Kneib, M. Limousin, Á. Elíasdóttir, P. J. Marshall, and T. Verdugo, New Journal of Physics **9**, 447 (2007).

J. F. Navarro, C. S. Frenk, and S. D. M. White, ApJ **490**, 493 (1997).

R. Kawamata, M. Oguri, M. Ishigaki, K. Shimasaku, and M. Ouchi, ArXiv e-prints, arXiv:1510.06400 (2015).

J. Liesenborgs, S. De Rijcke, and H. Dejonghe, MNRAS **367**, 1209 (2006).

J. Liesenborgs, S. de Rijcke, H. Dejonghe, and P. Bekaert, MNRAS **380**, 1729 (2007).

I. Mohammed, J. Liesenborgs, P. Saha, and L. L. R. Williams, MNRAS **439**, 2651 (2014).

H. C. Plummer, MNRAS **71**, 460 (1911).

A. Zitrin, T. Broadhurst, K. Umetsu, D. Coe, N. Benítez, B. Ascaso, L. Bradley, H. Ford, J. Jee, E. Medezinski, Y. Rephaeli, and W. Zheng, MNRAS **396**, 1985 (2009).

M. Postman, D. Coe, N. Benítez, L. Bradley, T. Broadhurst, M. Donahue, H. Ford, O. Graur, G. Graves, S. Jouvel, A. Koekemoer, D. Lemze, E. Medezinski, A. Molino, L. Moustakas, S. Ogaz, A. Riess, S. Rodney, P. Rosati, K. Umetsu, W. Zheng, A. Zitrin, M. Bartelmann, R. Bouwens, N. Czakon, S. Golwala, O. Host, L. Infante, S. Jha, Y. Jimenez-Teja, D. Kelson, O. Lahav, R. Lazkoz, D. Maoz, C. McCully, P. Melchior, M. Meneghetti, J. Merten, J. Moustakas, M. Nonino, B. Patel, E. Regös, J. Sayers, S. Seitz, and A. Van der Wel, ApJS **199**, 25 (2012).

A. W. Mann and H. Ebeling, MNRAS **420**, 2120 (2012).

L. Christensen, J. Richard, J. Hjorth, B. Milvang-Jensen, P. Laursen, M. Limousin, M. Dessauges-Zavadsky, C. Grillo, and H. Ebeling, MNRAS **427**, 1953 (2012).

J. Priewe, L. L. R. Williams, J. Liesenborgs, D. Coe, and S. A. Rodney, ArXiv e-prints (2016).

O. Yaron, D. Prialnik, M. M. Shara, and A. Kovetz, ApJ **623**, 398 (2005).

D. Prialnik and A. Kovetz, ApJ **445**, 789 (1995).

M. Kato, H. Saio, and I. Hachisu, ApJ **808**, 52 (2015).

J. Wambsganss, in *Gravitational Lensing: Recent Progress and Future Go*, Astronomical Society of the Pacific Conference Series, Vol. 237, edited by T. G. Brainerd and C. S. Kochanek (2001) p. 185.

C. S. Kochanek, ApJ **605**, 58 (2004).

B. Paczynski, ApJ **304**, 1 (1986).

C. Alcock, C. W. Akerlof, R. A. Allsman, T. S. Axelrod, D. P. Bennett, S. Chan, K. H. Cook, K. C. Freeman, K. Griest, S. L. Marshall, H.-S. Park, S. Perlmutter, B. A. Peterson, M. R. Pratt, P. J. Quinn, A. W. Rodgers, C. W. Stubbs, and W. Sutherland, Nature **365**, 621 (1993).

E. Aubourg, P. Bareyre, S. Bréhin, M. Gros, M. Lachièze-Rey, B. Laurent, E. Lesquoy, C. Magneville, A. Milsztajn, L. Moscoso, F. Queinnec, J. Rich, M. Spiro, L. Vigroux, S. Zylberajch, R. Ansari, F. Cavalier, M. Moniez, J.-P. Beaulieu, R. Ferlet, P. Grison, A. Vidal-Madjar, J. Guibert, O. Moreau, F. Tajahmady, E. Maurice, L. Prévôt, and C. Gry, Nature **365**, 623 (1993).

A. Udalski, M. Szymanski, J. Kaluzny, M. Kubiak, W. Krzeminski, M. Mateo, G. W. Preston, and B. Paczynski, ACTAA **43**, 289 (1993).

K. Chang and S. Refsdal, Nature **282**, 561 (1979).

K. Chang and S. Refsdal, A&A **132**, 168 (1984)